Author version: *Geochim. Cosmochim. Acta, vol.99; 2012; 110-127*

Fractionation and fragmentation of glass cosmic spherules during atmospheric entry

N.G. Rudraswami[1*], M. Shyam Prasad[1], E. V. S. S. K. Babu[2], T. Vijaya Kumar[2], W. Feng[3], and J. M. C. Plane[3]

[1]National Institute of Oceanography (Council of Scientific and Industrial Research), Dona Paula, Goa 403 004, India

[2]National Geophysical Research Institute, (Council of Scientific and Industrial Research), Hyderabad 500 007, India

[3]School of Chemistry, University of Leeds, Leeds LS29JT, UK

*Corresponding author: rudra@nio.org

Abstract

Glass cosmic spherules are a sub–type of S–type cosmic spherules that are almost at the end phase of fractionation and volatilization during atmospheric entry. A focused investigation of 36 glass spherules out of several hundred spherules reveals fractionation and fragmentation phenomena. During atmospheric entry, some of the glass spherules largely preserve relict pyroxene normative crystals within. The spherules appear to have experienced temperatures of ~1700^{o}C that resulted in vaporization of Fe and other volatile elements such as S, Na and K from the silicate spherule, resulting in the enrichment of SiO_2, MgO, and CaO in weight percent. Calculations with a chemical ablation model suggest an entry velocity of ~11–16 km/s to achieve the temperature required for glass spherule formation under these conditions the micrometeoroid undergoes a mass of loss of ~ 20%. Any increase in entry velocity will increase the mass loss drastically and change its chemical composition. Most glass spherules beyond a certain threshold diameter of ~300 μm appear to undergo fragmentation resulting in two different spherules, which could lead to an apparent enhancement of the percentage of glass spherules in unbiased collections. Siderophile and volatile element loss and subsequent development of a platinum group element (PGE) nugget are observed in one of the spherules. This appears to be the first reported observation of a platinum group nugget (PGN) in a glass spherule. The nugget has a diameter of ~ 3 μm and contains all the six PGE, although some of the more volatile PGE are depleted relative to an average chondritic composition. Interestingly, the PGE data of the nugget seem to have a trend which is similar to that of a PGE nugget from a Calcium Aluminium rich Inclusion (CAI). The trace element data of these glass spherules suggest that their parent bodies were carbonaceous chondrites.

1. INTRODUCTION

Micrometeorites collected from the Earth and stratosphere in the size range of few tens of micrometers to a millimeter with the peak of the mass distribution around a diameter of ~200 μm provide important information for understanding the formation of the solar system (Blanchard et al., 1980; Maurette et al., 1986, 1991; Love and Brownlee, 1991, 1993; Bland et al., 1996; Ceplecha et al., 1998; Taylor et al., 2000; Rubin and Grossman, 2010). Most of the cosmic dust grains that reach the earth's surface come from carbonaceous chondrites (Kurat et al, 1994; Engrand and Maurette, 1998; Genge and Grady, 2002), whereas the majority of larger meteorites (~87%) are ordinary chondrites (Krot et al., 2003). Furthermore, out of an annual flux of ~40,000 tons of micrometeoroids that impact on the upper atmosphere, the majority (>90%) are ablated (Vondrak et al., 2008). Finally, the material that survives and reaches the earth surface is ~3000 tons yr^{-1} (Love and Brownlee, 1993; Taylor et al., 1998; Peucker-Ehrenbrink and Ravizza, 2000). Some of the smaller dust particles called interplanetary dust particles (IDPs) are collected in pristine form from the stratosphere (Brownlee et al., 1985). For surviving atmosphere entry, size plays an important role in combination with chemical composition, physical structure, entry velocity and entry angle (Brownlee, 1985; Love and Brownlee, 1991, Vondrak et al., 2008). All micrometeorites ≤ 50 μm are expected to survive the rigors of atmospheric entry with the exception of the particles having high velocities and low zenith angles (Love and Brownlee, 1991; Vondrak et al., 2008). Larger micrometeorites have undergone ablation leading to siderophile and volatile element depletion, and mass loss resulting in the relative enhancements of the more refractory components. Based on the relative amounts of volatilization observed, S-type spherules are sub-divided into scoriaceous, relict grain bearing, porphyritic olivine, barred olivine, cryptocrystalline, glass and Calcium Aluminium Titanium-rich (CAT) (Taylor et al., 2000; Genge et al., 2008). In this scheme, scoriaceous spherules have undergone partial melting, and CAT spherules, which contain high amounts of the refractory elements Ca, Al, and Ti are the most depleted in volatiles and siderophile elements. Out of the above, glass cosmic spherules (> 100 μm in size) constitute between ~ 15–22% of the total micrometeorite flux in unbiased collections (Maurette et al., 1986; Harvey and Maurette, 1991; Taylor and Brownlee, 1991; Taylor et al., 2000). Therefore, a substantial population of the sub-mm meteoroids that enter the earth are partly volatilized and transformed into glass spherules, and these are almost at the final stage of volatilization and vaporization of the parent meteoroid body. Most spherules are suggested to have chondritic bodies as precursors and have undergone evaporative losses during atmospheric entry (Brownlee, 1985; Brownlee et al., 1997; Engrand and Maurette, 1998; Herzog et al., 1999; Genge and Grady, 2002; Engrand et al., 2005; Yada et al., 2005; Cordier

et al., 2011b). However, more recently a small population of glass spherules was identified that could have achondritic parent bodies (Taylor et al., 2007; Cordier et al., 2011a).

For the present study we collected large sized (≥200 μm) cosmic spherules by sieving massive quantities of deep sea sediments from the Central Indian Ocean. Out of the 481 spherules that were isolated, 36 are glass spherules. A few of these glass spherules show effects of fragmentation and formation of crystals within the spherules. In addition, one glass spherule reveals the formation of a platinum group nugget (PGN) as large as ~3 μm in size, while PGNs have been described usually in I-type spherules and a lone barred spherule (Brownlee et al., 1984; Bonte et al., 1987; Rudraswami et al., 2011). This is perhaps the first time that a PGN is observed in a glass spherule as a possible effect of the processes undergone during atmospheric entry. A recently developed Chemical Ablation Model (CABMOD) (Vondrak et al., 2008) is then used to predict the likely meteoroid entry velocities, which give rise to the observed differential ablation of the elemental constituents. The present investigation therefore highlights the processes that lead to the formation, fractionation and fragmentation of glass spherules.

2. SAMPLES AND ANALYTICAL TECHNIQUES

2.1 Sampling techniques

We collected sediment samples from the deep sea floor using a grab sampler during a grid sampling operation in the Central Indian Ocean for manganese nodules. The total sediment recovered at each location varied from 20−40 kg, and the sediment type was siliceous ooze. The sediments recovered were sieved on board of the Akademik Aleksandr Sidorenko (research vessel chartered by the Government of India), cruise number 38 during May-June 2001. A sieve having a mesh size of 200 μm was used for wet sieving onboard. The fraction ≥200 μm was dried and magnetically separated; the separates were examined under a binocular microscope and the spherules were handpicked. In all, 481 spherules of diameters ≥200 μm were characterized from ten samples after sieving ~300 kg of sediments, around 11% of all the spherules were glass type. The spherules were initially observed under the optical microscope, subsequently mounted in epoxy and polished sections were obtained. Spherules with an unusual appearance under the optical microscope were initially observed unpolished in a scanning electron microscope and were subsequently polished for analyzing their internal features.

2.2. Electron microscopy

All the spherules were initially observed using an optical microscope and later with a scanning electron microscope (SEM, JEOL JSM 5800LV) at the National Institute of Oceanography,

Goa. Identification of the textural features, classification and characterization of the polished sections were initially done in the SEM by observing the back scattered electron (BSE) and secondary electron (SE) modes. An OXFORD-INCA energy dispersive spectrometer detector (EDS, ISIS-300) linked to the SEM with a Ge detector was used for initial identification and quantitative elemental analysis of phases in the spherules. Olivine from the Springwater meteorite (USNM-2566) and hypersthene from the Johnstown meteorite (USNM-746) (Jarosewich et al., 1980) were used as standards for the analysis of silicate portions. The EDS was also suitable for analysing the micrometer-sized platinum group nugget (PGN) present in one of the glass spherules, AAS-38-175-II-P2. For platinum group element (PGE) measurements, pure elemental (99.9%) standards were used. The INCA software energy uses the XPP matrix correction to process the results (Pouchou and Pichoir, 1991). The L and M series lines were used for the platinum group elements. The electron microprobe beam is a few μm in size, which precluded analysis of the nugget in view of its small diameter. The SEM beam was focused on the centre of the nugget to avoid scatter from the neighbouring surface. Multiple analyses were made to verify repeatability. The uncertainty in the EDS analysis depends on the concentration of the element present in the nugget. Generally, for an elemental concentration greater than 7 wt%, the uncertainty is less than 10 relative-%. However, the error percentage raises significantly to ~20% for low concentration elements like Pd and Rh.

The bulk and spot quantitative analyses on all the glass spherules for major elemental compositions (Na_2O, MgO, Al_2O_3, SiO_2, CaO, TiO_2, Cr_2O_3, MnO, FeO and NiO) were done on plane surfaces in the polished sections using the CAMECA SX-100 (Physical Research Laboratory, Ahmedabad) and CAMECA SX-5 (National Institute of Oceanography, Goa) electron probe micro analyzer (EPMA) equipped with three and four wavelength-dispersive spectrometers, respectively. The element such as S, P and K measured were below the detection limit. The instrument parameters for the bulk analysis are as follows: ~15 μm beam size, beam current of 12 nA and accelerating voltage of 15kV. Multiple analyses were done to improve the analytical precision of the bulk analysis (**Table 1**). The spot analysis on the mineral phases was conducted with a beam diameter of ~1−2 μm, with the other parameters fixed (**Table 1 and 2**). Data reduction and correction were performed using PAP with an online program (Pouchou and Pichoir, 1991).

2.3. Trace element analyses

Subsequent to SEM and electron microprobe analysis, in-situ trace element analysis on polished thick sections of 15 glass spherules was carried out using a New Wave UP213 nm Laser Ablation system coupled with a Thermo X Series^{II} inductively coupled plasma mass spectrometer (LA-ICP-MS) at the CSIR-National Geophysical Research Institute (NGRI), Hyderabad. An

aperture-controlled 40-60 μm focused Nd:YAG laser beam on a continuous mode for an ablation time of 80 to 120 seconds with a repetition rate of 10 Hz (10 pulses per second) gives an energy of ~2.5 mJ. A thick polished bead of NIST SRM 612 was used as a running standard during the spherule analyses. Measurements on 8 spot analyses (chosen through BSE images) were bracketed by 4 analyses of SRM 612. BCR-2G (US Geological Survey) was used as an internal standard before every analysis run. The ablated sample was extracted in a He-environment using a Large Format Cell (LFC) of the New Wave UP213 LA System and then mixed with Ar nebuliser gas before being introduced into the plasma of the ICPMS. The ICPMS was tuned using SRM NIST 612 glass to achieve a sensitivity of $^{139}La > 5000$ cps/ppm and $^{238}U > 12000$ cps/ppm while keeping the $ThO/^{232}Th < 1\%$. The nebuliser gas flow rate was 0.75 L/min and the He flow rate was 0.6 L/min. The time-resolved analysis data was processed off-line using the 'Glitter' software obtained from Macquarie University, Australia. A 45s gas blank and 85s integration time was used for each analysis run with a purge time of 35s at the end of each run.

3. RESULTS

3.1. Terrestrial age of spherules

The surface sediment samples from which the spherules are extracted have been collected from an area which is approximately 200 km × 100 km in the Central Indian Ocean. We took ten samples between the locations : Lat $10^0$30' – $12^0$30'S and long $74^0$30 – $75^0$45'E. The grab sampler penetrates to a maximum of 15 cm below the seafloor with a total collection capacity of ~50kg wet sediment. For a seafloor depth of 15cm, the spherules in the sediment would have terrestrial ages of 0–50,000 years based on the rates of sedimentation in the area. This age arrived is based on the core depth at which the well-dated Australasian microtektite peak at 0.77 Ma is observed (Izett and Obradovich, 1992; Kunz et al. 1995); the horizon containing microtektites of this impact have been found over almost the entire Indian Ocean in several sediment cores (Glass and Koeberl, 2006; Prasad et al., 2007). We have also collected three long (~6m) cores in this area, in addition to the surface sediment samples, which contained Australasian microtektites of 0.77 Ma age. From the ten surface sediment samples that are examined for this study, 481 cosmic spherules are isolated. Due to the vast range in their residence times on the seafloor, the spherules show a range of etching/weathering from very well preserved (i.e., almost unetched) spherules to those which have been destroyed by the process of etching. Of the different types of spherules, the barred ones show maximum etching where the glass portion between the olivine bars of some spherules have been almost completely etched out and the I-type spherules from the collection show the least etching. The glass spherules in general show lower levels of etching.

3. 2. Petrology and chemistry of glass spherules

The mineralogy and major element compositions of selected glass spherules are summarized in **Table 1**. The glass spherules observed in the present collection (**Fig. 1–5**) have three distinctive morphologies:

(a) Some glass spherules have smooth and spherical external features. The polished sections also resemble the externally observed features (**Fig. 1a, d, f**). They occasionally contain large vesicles similar to those described by Taylor et al. (2007, 2012) (e.g. AAS-38-178-#1-P8, **Fig. 1a**; AAS-38-178-II-P16, **Fig. 1f**). These have relatively small diameters and display only one type of texture – which can be either plain, or swirling. The swirling textures were suggested by Taylor et al. (2012) to be a product of extensive heating and transformation of coarse-grained micrometeorites during atmospheric entry.

(b) A number of glass spherules have a scalloped appearance. Some of these spherules are composed of many grains observable in the polished sections (**Figs. 1b and c**). These crystalline features appear to be in various stages of development. Also found in this category are those with a scalloped appearance having smooth glass interiors (**Figs. 1d and e**). Glass spherules with a scalloped appearance have been reported earlier by Taylor et al. (2007). They suggested this appearance results from a high degree of etching. Some of these spherules contain a mixture of cryptocrystalline and glass textures, where the glass textures are marked by the development of crystals whose boundaries range from diffuse to well-defined (**Fig. 2–4**). The scalloped appearance seems to be due to Si-rich, frothy, exterior glassy layers formed on these spherules as described in the section below. These types of spherules are the fragmented halves of larger glass spherules as described below.

(c) Large glass spherules having diameters ≥250 μm and elongated shapes. A constriction is observed in the mid-portion of some of these spherules which appear to be breaking apart into two different spherules (**Fig. 2–3**). More importantly, some of these spherules have an Fe and/or Ni rich cap forming as a thin layer on one side of the spherule (**Fig. 3**). The metal constituents are at all stages of being ejected from the spherules (e.g. **Fig. 2d, 3c–d**). In some of the spherules, crystallization centres have grown inside with the development of sub-hedral pyroxene normative crystals (**Fig. 4a–b**). In these spherules fissures are observable which could have been leading to fragmentation (**Fig. 2 and 3a–b**). An individual spherule can display two different textures: one part having an amorphous texture and the other part a crystalline texture **(**e.g**. Fig. 2i**). With continued heating, Fe–Ni enters the oxide phases leaving behind the most noble platinum group elements to

form into a nugget at the earth-facing side of the spherule **(Fig. 5)**. The external surfaces of all the large glass spherules exhibit structures which are either flow lines or crystallization patterns **(Fig. 5c)**.

A rim in few spherules is either frothy, or smooth and continuous, in appearance (**Fig. 2–3)**. Also, the metal contained in the spherule segregates into a Fe-Ni bead due to frictional heating during entry and pyrolysis (Brownlee and Bates, 1983), and is ejected as a bead. Because of the low vaporization temperature of sulphur, all of it is vaporized from the spherule (**e.g. Fig. 3c–d**).

The Taylor et al. (2000) collection showed that 17% out of 1588 spherules of >50 μm from Antarctica are glass spherules. However, this percent rose dramatically (~45%) for spherules that are >250 μm in diameter (e.g., Fig. 3 of Taylor et al. (2000)). Further, 5% of the spherules were found to be highly vesicular and 7% had one or more Fe-Ni beads (Taylor et al., 2000). Importantly, they went on to suggest that small Ni-rich metal beads were probably a transitional phase between Fe-Ni metal beads and platinum group nuggets. Spherules of all the above types described by Taylor et al. (2000) are found in the present collection in addition to the spherules having pyroxene crystals (**Fig. 1–2**).

A single glass spherule AAS-38-176-II-P16 (**Fig. 1f**) shows the presence of a relict chromite grain which measures 40 × 20 μm. This chromite grain has chemical composition as follows: Cr_2O_3 ~55.1wt%, FeO ~26.2wt%, MgO ~ 7.4wt% and Al_2O_3 ~ 5.9wt% (**Table 2**).

3.3. Chemical Compositions of the phases in glass spherules

Externally, a large number of glass spherules contain either a Si-rich glass or Fe-Ni rich cap over their surfaces. In some spherules a Fe-Ni bead appears to be in the final stages of being ejected. For example, the Fe-Ni rich phase at the tip of AAS-38-182-P4 (**Fig. 2d**) has a composition of NiO ~64.1wt%, FeO ~16.3wt%, SiO_2 ~14.9, Al_2O_3 ~ 1.9 wt%, and CoO ~0.7wt%. Whereas in AAS-38-186-P1 (**Fig. 3c**), there is a Fe-Ni metal bead at the tip of the spherule, and a Fe-Ni cap covers ~30% of the spherule. The size of the bead as well as the thickness of the Si–rich cap varies. AAS-38-77-P3 with a scalloped appearance (**Fig. 3d**) contains frothy cavities on its surface. The scalloped portion has a higher Si contents than the spherule interiors. The Si-rich cap is also seen in the polished section of AAS-38-77-P3 (**Fig. 2g**).

BSE images of three glass spherules (AAS-38-175-II-P2, AAS-62-54-#1-P1 and AAS-62-54#2-P27) show the presence of mineral grains in the polished section (**Fig. 4** and **Table 2**). The presence of such crystals in the interior is observed only in the large glass spherules. The chemical composition of the mineral grains suggests low-Ca pyroxene, this composition is no different from

that of the bulk composition of the spherule which basically means the crystals are growing in a pyroxene normative melt. In AAS-38-175-II-P2, crystal formation can be seen in one half of the spherule (**Fig. 5a**), this is also visible in the polished section (**Fig. 5b**). Similar behaviour of crystal formation is also seen in AAS-62-54-#1-P1 (**Fig. 2h**) and AAS-62-54#2-P27 (**Fig. 2i**), whose enlarged view is shown in **Fig. 4**. The elemental composition of the mineral grains is given in **Table 2**.

Some of the spherules have glass caps enveloping their surfaces. Morphologically, these caps are similar to the ones shown by Taylor et al. (2000). The chemical compositions of the parts enveloped by glass caps are given in **Table 2**. **Fig. 3a** and **b** are optical microscopic images of AAS-62-54-#1-P1 and AAS-62-54-#2-P27 that show the presence of fissure development in the spherules and also the presence of a glass cap. Whole spherule BSE images of AAS-38-186-P1 (**Fig. 3c**) and AAS38-77-P3 (**Fig. 3d**) show the presence of glass caps along with Fe-Ni beads on these spherules. The spherules AAS-38-186-P1 and AAS38-77-P3 appear to have Fe-rich and Si-rich caps, respectively. This type of cap is clearly visible in the polished section in AAS-38-147-I-P2 (**Fig. 2f**) where a continuous layer of Si-rich cap surrounds the spherule. AAS-38-77-P3 has a Si-rich cap around the spherule as can be seen in **Fig. 2g**. The glass cap in AAS-38-77-P3 is enriched in SiO_2 by ~20wt% and Al_2O_3 by ~3wt%, while the MgO content is reduced by ~ 25wt% compared to the bulk spherule content as shown in **Fig. 6** and given in **Table 2**. These compositions and the presence of K and Na on these caps suggest that the glass caps could be due to hydration of the glasses while on the seafloor. There have been several investigations on the behaviour of glasses and spherules on the seafloor. Glass et al. (1997) investigated the hydration of glasses of tektite composition (Si-rich glasses) of ages 0.77 Ma to ~35 Ma; and also clinopyroxene spherules that belong to an impact layer of ~35 Ma age. They find that the hydration increases linearly with age. On glasses of tektite composition it is difficult to identify the effects of hydration. It is seen more often in the low totals obtained in the electron microprobe analysis. A more dependable test was to heat the samples up to 1100^0 C and they are seen to froth – a tektite which is not hydrated would not froth upon heating. For CPX spherules (which are closer in chemistry to the glassy spherules in the present study), they found a large scale reduction in all the major oxide contents with an increase in the K and Na contents of the rims of the glasses that had undergone hydration. The glassy spherules in the present study have compositions which are Fe-Mg rich and are closer to basaltic compositions rather than Si-rich tektites. The hydration and palagonitisation of basaltic glasses has been actively investigated for several decades. Thorseth et al.'s (1991) detailed investigations on basaltic glasses have clearly shown that there is a depletion of all oxides except for Si and Al leading to relative enrichment of

these two oxides. This is also accompanied by alkali enhancement seen as increased percentages of Na and K in the hydrated/weathered zones of basaltic glasses.

In view of the above, the glass caps/rims if they are generated during the descent of the spherules through the atmosphere, have experienced selective leaching of the other major elements leading to the relative enrichment of Si and Al. Or they are the result of hydration during their residence times on the seafloor.

Taylor et al. (2000) described glass cap spherules in their Antarctic collection mostly on glass and barred olivine spherules. Further, some of the glass caps were found to be Fe-rich because of migration of metals during bead formation. Taylor et al. (2000) also presented analytical data for 169 such glass spherules that have SiO_2 compositions within the range of the present study, while the MgO contents are lower and the FeO contents are much higher in our samples (**Table 1**).

The bulk chemical composition of glass spherules shows depletion in the abundances of elements such as Na and Cr compared to chondrites/ achondrites, which is likely due to the evaporative loss of these elements during atmospheric entry (**Fig. 7**). However, the bulk chemical compositions of Al, Ca, Mg, Fe are generally CI-like except for some volatile elements, which rules out an achondritic parent body. Taylor et al. (2007) reported anorthite with low Mg contents in glass spherule SP37-3 which they suggested is similar to the anorthite in achondrites rather than in chondrules from chondrites. The low Mg content in anorthite may be the result of an artefact of secondary disturbance during atmospheric heating. This type of low Mg content in feldspathic phases has also been reported earlier in chondrules of least metamorphosed chondrites (Russell et al., 1996; Kita et al., 2000; Rudraswami et al., 2008).

3.4. The nugget-bearing glass spherule AAS-38-175-II-P2

The most 'evolved' of the spherules AAS-38-175-II-P2 has a smooth surface texture, does not have a Fe-Ni bead, but possesses a PGN at the front end. The SE image of the exterior and BSE images of the polished surfaces of AAS-38-175-II-P2 are shown in **Fig. 5**. This spherule AAS-38-175-II-P2 is bullet–shaped (semi–major axis of ~260 μm and semi–minor axis of ~200 μm) and appears to have striations or crystallization patterns. The aft portion of the spherule appears to develop into crystals of orthorhombic shapes. Internally, there seems to be a boundary between these two 'segments' of the spherule (**Fig. 5b**), from which a furrow seems to be developing which, with more ablation, would have eventually have caused the spherule to separate into two parts. Also, AAS-38-175-II-P2 does not have scalloped portions but is smooth throughout with a glassy cover

that envelops most of the spherule. The interior and crystal compositions are listed in **Table 1 and 2,** respectively.

The nugget side of spherule has the appearance of a barred texture at high magnification (**Fig. 5c**). The nugget has a diameter of ~3 μm and is nearly spherical. A magnified view of the nugget is presented in **Figs. 5c and d**. The platinum group element (PGE) composition in the nugget is not homogenous as can be seen in **Table 3**, which is unlike the nuggets reported in I-type spherules (Brownlee et al., 1984; Bonte et al., 1987; Rudraswami et al., 2011). Bonte et al. (1987) has reported heterogeneity in nine nuggets (<1 μm in size) found in a single barred olivine spherule. All nine nuggets had PGE with different compositions and were therefore termed "disequilibrated". The nugget in AAS-38-175-II-P2 appear to be two hemispheres with differing compositions. The portion marked '2' in **Fig. 5d**, which is the inner half, contains all six PGE but in smaller quantities than the portion marked '1' (which is the outer half). In addition, both these hemispheres contain appreciable quantities of Fe and Ni (**Table 3**).

3.5. Trace element studies of glass spherules

The trace element geochemistry of glass spherules obtained using the LA-ICP-MS normalized to CI (Lodders and Fegley, 1998) is plotted in **Fig. 7**. The trace element data are close to CI chondrites, as shown by the dark thick line which is the average data from 12 spherules (the data from 3 other spherules are not included as they exhibit a large variation from chondritic). The trace elements do not seem to show much fractionation and behave as a single group with respect to CI chondrites. If one considers a CI-chondrite-like parent body, there would be considerable compositional heterogeneity in the spherules. Here, the refractory elements (right hand side of **Fig. 7**) seem to have mobilized and homogenized easily within the spherules, but have not evaporated, which otherwise would have led to significant fractionation. The concentration of the trace elements Zr, Hf, Y, Lu, Er, Ho, Tb, Tm, Dy, Gd, Nd, Sm, Pr, La, Yb, Ce, Eu and Sr in these spherules is ~1.6× CI chondrites, while that of Sc, Th, Ta, Nb and Ba is ~2.2× CI chondrites. The U content is slightly depleted, 0.7× CI chondrites, compared with the more highly depleted elements Co, Rb, Zn and Pb which are <0.4× CI chondrites. Volatility does not seem to have affected the majority of the trace elements, implying that large scale heating leading to significant modification in the concentration of the more refractory elements has not been taken place.

4. DISCUSSION

Love and Brownlee (1993) suggest a micrometeorite flux of ~40,000 tons/yr with an average micrometeorite diameter of ~200 μm, based on particle impact detection on their Long Duration

Exposure Facility (LDEF), which was in low earth orbit for about 6 years. Estimates of the terrestrial flux based on recovered micrometeorites are widely debated and not well constrained. There is a wide range of flux estimates from ~2700 tons/yr (Taylor et al., 1998), 5300 tons/yr (Duprat et al., 2006) and 11000–16000 tons/yr (Yada et al., 2004) from polar collections. Essentially, this difference in the collected material and estimates based from the detector in space indicates that a major portion of the extraterrestrial particulate matter is vaporized during atmospheric entry (Yada et al., 2005; Vondrak et al., 2008). Therefore, glass spherules that constitute a sizable fraction of the collection (~15–22% of total recovered micrometeorites) form a substantial component of the recovered particulate extraterrestrial matter on earth, and are dust particles that have experienced close-to-maximum heating during atmospheric entry, next only to CAT spherules (Taylor et al., 2000). Our discussion of the glass spherules in the present study will cover the formation and pre-atmospheric size of a particle, the fractionation of the elements during ablation, volatilization of Fe and other more volatile elements, formation of a platinum group nugget, and the presence of a crystalline phase. Here, we have made use of the chemical ablation model (CABMOD) to put constraints on the formation of glass spherules during atmospheric entry (Vondrak et al., 2008).

4.1. Significance and origin of platinum group nuggets in glass spherules

Platinum group nuggets were first discovered in I-type spherules (Brownlee et al., 1984), and were subsequently found in a single barred olivine spherule (Bonte et al., 1987). More recently nanometer- and micrometer-sized nuggets were reported by Rudraswami et al. (2011) in I-type spherules. The platinum group nugget of ~3 μm size in AAS-38-175-II-P2 (from the present study) is the largest found so far in S-type spherules. Rudraswami et al. (2011) reported the process of fractionation of PGE within I-type spherules, where the more refractory PGE (Os, Ir) were associated with μm-sized nuggets and the more volatile PGE (Pt, Rh and Pd) were associated with the hundreds of nm-sized nuggets that are distributed throughout the I-type spherules. The most volatile element among the PGE is Pd, which all investigators have reported to be depleted in I-type spherules, except for one out the ten nuggets investigated by Brownlee et al. (1984). Furthermore, the PGE distribution in the nuggets suggested a fractionation pattern that could have resulted from the heating and oxidation of a chondritic parent body (Brownlee et al., 1984; Rudraswami et al., 2011). However, the nuggets reported in the S-type spherule by Bonte et al. (1987) had different compositions which did not indicate any known pattern, and these nuggets were suggested to be ‘disequilibrated’. Interestingly, high concentrations of Pd were reported in one such nugget. Further, there are very few analyses of PGNs in ordinary chondritic meteorites and many are usually

associated with CAIs in carbonaceous chondrites (Grossman and Ganapathy, 1976; Palme and Wlotzka, 1976; Palme, 2008). Palme and Wlotzka (1976) analyzed a metal particle in one Allende CAI that was enriched in platinum group elements and some ratios among these elements (Ru/Ir, Pt/Ir, Rh/Ir, Pt/Rh, and Ru/Os) were found to be close to CI values. The PGE–rich metal was suggested to be an independent condensate that was later incorporated into the CAIs (Grossman and Ganapathy, 1976). Nuggets observed in the CAIs of carbonaceous chondrites were termed as 'primary' and have been assigned an interstellar/presolar origin (Palme and Wlotzka, 1976). The analyses that are available for the nuggets in CAIs show a high degree of heterogeneity in the PGE concentrations. However, the bulk PGE content of carbonaceous chondrites, which is a sum of all nuggets and PGE present in the CAIs, chondrules and all other sub-components, is close to CI values (MacPherson, 2003; Tagle and Berlin, 2008). The nugget in the present study has a heterogeneous siderophile element composition indicating that the heating time required for homogenization of the PGE may not have been sufficient. Also, the silicates in AAS-38-175-II-P2 may not have been completely stripped of their PGE during the process of nugget formation (if we consider that the nugget formed as a result of segregation during entry), or after the nugget formed it cooled rapidly, preventing homogenization. The nugget in the present study has PGE ratios which match closely with the corresponding ratios in CAI data from the Allende chondrite (Palme and Wlotzka, 1976) (**Fig. 8** and **Table 4)**. For example: Os/Ir (0.55 and 0.55), Ru/Ir (1.02 and 1.34), Rh/Ir (0.34 and 0.22), Pt/Ir (2.43 and 1.62), Pt/Rh (7.13 and 7.71) and Ru/Os (1.88 and 2.42) where the first ratio in parenthesis is from the CAI of Allende (Palme and Wlotzka, 1976) and the second ratio is from the present study. Slight volatilization of Pt and Rh has led to a decrease in other ratios such as Pt/Ir, Rh/Ir, Pt/Os, and Pt/Ru. The Os/Ir ratio of different chondritic meteorites (CI, H, L, LL, L/LL, EH, and EL; Tagle and Berlin, 2008), one CAI in the Allende (Palme and Wlotzka, 1976), iron meteorites (Pernicka and Wasson, 1987; Campbell and Humayun, 2005), I-type cosmic spherules (Brownlee et al., 1984; Bonte et al., 1987; Rudraswami et al., 2011) along with AAS-38-175-II-P2 are shown in **Fig. 9**. The nugget in AAS-38-175-II-P2 has Os/Ir falling close to the CAI data of the Allende chondrite. The majority of the nugget data from I-type spherules falls near the chondritic value; however, due to the spread in some data (Brownlee et al., 1984; Bonte et. al., 1987; Rudraswami et al., 2011) one cannot conclusively rule out iron meteorites as precursors for the I-type spherules (Brownlee et al., 1984; Bonte et al., 1987). Based on Cr/Fe and Fe/Ni ratios, Herzog et al. (1999) concluded that I-type spherules originated from meteoritic metals of CO, CV, CR and unequilibrated ordinary chondrites. Similarly, based on the chemical and isotopic studies of cosmic spherules many researchers concluded that a majority of the spherules have carbonaceous chondrite precursor material (Brownlee et al., 1997; Engrand et al., 2005; Cordier et al., 2011c). This may be an

indication that the majority of glass and I-type spherules have chondritic precursors, whereas I-type spherules are also the result of differentiation during atmospheric entry. Overall, the nugget seems to have escaped major vaporization and total chemical homogenization during its evolution thereby retaining some primary signatures which indicate the possibility of a connection to relict grains in CAIs.

The presence of palladium content (~2–6%) in the nugget suggests that the peak temperature experienced by this glass spherule during formation is less than ~1700^{o}C during formation, although the elemental ratios of Pd/Pt and Pd/Ir point towards volatilization of palladium (**Table 4**). Further, different compositions of two parts of the same nugget also imply unfractionated PGE composition in the nugget compared to chondritic/CAI values. Among the various stages of melting of spherules olivine normative compositions are observed at the barred olivine, cryptocrystalline stages; whereas with increasing heating of the same parent body glass spherules result with the evaporation of Fe. The temperatures that are needed to attain this stage could be anywhere between 1700 and 2000^{o}C, especially if one considers the forsterite melting temperature of 1900^{o}C (Deer et al., 1992). Further, Deer et al. (1992) observed that under conditions of equilibrium crystallization from liquids containing between ~43wt% and ~60wt% SiO_2, the early formed forsterite reacts to form enstatite in this temperatures range (1700–2000^{o}C).

The major elemental ratios also illustrate progressive heating and volatilization. For example, the Fe/Si ratio of AAS-38-175-II-P2 that contains the PGN shows greater volatilization of Fe than the other spherules (**Table 5**). With further heating and increased oxidation as the micrometeoroid penetrates deeper into the atmosphere, the most refractory and noble elements appear to start segregating into nuggets, following the process defined by Brownlee et al. (1984). The segregation takes place in an olivine normative medium in the melt, where the nugget can form more efficiently due to the high partition coefficient of metal/silicate (Brenan et al., 2005). The concentration of the PGE is dictated by silicate–metal partitioning. The PGE that are not compatible with silicate get released from the silicate melt due to their high metal/silicate partition coefficients ($D^{met/sil}$ of Pt >10^{15}, Rh >10^{9} (Ertel et al., 1999), Pd ~10^{7} (Borisov et al., 1994), Ir~10^{9}–10^{12} (O'Neill et al., 1995; Brenan and McDonough, 2009), Os~10^{9}–10^{12} (Brenan and McDonough, 2009)). These large partition coefficients help the PGE in the melt to accumulate and segregate as a nugget as suggested by most of the above simulation experiments. The amount of fractionation will depend on various factors such as temperature, heating time, partition coefficients of the elements, and oxygen fugacity (Borisov & Palme, 1995, 1997). However, to grow to a size of ~3 μm, a considerable concentration of PGE needs to be available in the parent body of the spherule. The concentration of

PGE can be used to estimate the size of the spherule parent body before its entry into the atmosphere. Assuming that the Os concentration in the nugget is distributed uniformly, and that the Os concentration in chondrites is ~500ng/g, the minimum size of the spherule before atmospheric entry is estimated to be ~1.2 times the present size by volume. The implied ~20% mass loss in the silicate body is much smaller when compared to that experienced by I-type spherules (Rudraswami et al., 2011). Also it is important to note that an extremely low concentration of PGE is expected to be preserved in silicate after segregation, because of its strong siderophile nature and consequent partitioning into the nugget (Palme, 2008).

The Mn–Mg–Fe systematics for all the glass spherules fall within the chondritic range (**Fig. 10**). Taylor et al. (2007) reported on glass spherules that appeared to have a HED (howardite, eucrite, and diogenite) parent body, we have not encountered spherules of this type in the present collection. A chondritic parent body is also supported by Ca/Si versus Al/Si, which fall near to the solar values for all the glass spherules (**Fig. 11**). The elemental ratios such as Mg/Si, and Ca/Si (**Table 5)** of AAS-38-175-II-P2 and other glass spherules from the present study provide support for a carbonaceous chondrite as the parent body, while the other ratios are disturbed.

4.2. Fragmentation and ablation of glass spherules

From observing 36 glass spherules, it appears that the spherules with sizes >300 μm have a greater chances of breakup as they interact with the earth's atmosphere at altitudes of ~80-120 km. This is visible in AAS-62-54-#1-p1 and AAS-62-54-#2-p27 shown in **Fig. 2h and 2i**, respectively. The frictional force generated by collisions with air molecules (mostly N_2 and O_2) is not adequate to fragment large particles at altitudes greater than ~120 km, however, if sufficient water was trapped inside a particle then formation of superheated steam might cause fragmentation at relatively low particle temperatures, corresponding to higher altitudes (E. Murad, Air Force Geophysics Laboratory, pers. comm.). As the micrometeoroid descends below 120 km the force can become sufficient to fragment the incoming particle. AAS-62-54-#2-p27 is an example of imminent fragmentation into two spherules. The production of micrometeorites by fragmentation is also supported by the Lal and Jull (2002) model. They suggested that most micrometeorites are produced by fragmentation, although this proposal is not completely supported in the present study. The heating and cooling of a micrometeorite is complete within ~10–15 seconds (Love and Brownlee, 1991). By the time a micrometeorite decelerates to velocities < 3 km/s, and the temperature is below ~900^{o}C, it is already a solidified object.

Fragmentation depends on various factors such as size, angle of entry and entry velocity, as well as the chemical composition of the incoming particle. The S-type spherules with low density do not penetrate deep into the atmosphere and are largely ablated due to their high ablation coefficients (Janches and ReVelle, 2005). Fragmentation is of no major consequence for smaller (<100 μm) particles. But as larger particles enter the atmosphere, it get heated for longer time, some of them may undergo strong deformation leading to fragmentation or breakup. Furthermore, the incipient nuclei of crystallization are preserved within a melt with a composition similar to that of bulk spherule. Many of the fragmented spherules show evidence of being part of a larger spherule in the form of scalloped appearances and development of crystals, which have been observed on unfragmented larger spherules. Therefore, in order for a spherule to fragment, the precursor meteoroid material needs to be of large dimensions (>300 μm). Fragmentation of these large particles will then lead to an increase of spherules in the size range ~150–200 μm, an indication of which is seen in **Fig. 12**.

We now use the Chemical Ablation Model (CABMOD) (Vondrak et al., 2008) to quantify some of these effects. In CABMOD, the particle velocity, entry angle, density and mass are first specified. The model then treats the following processes: sputtering by inelastic collisions with air molecules before the meteoroid melts; frictional heating of the particle until it melts, at which point atoms and oxide molecules evaporate from the molten meteoroid. Thermodynamic equilibrium is assumed between the particle (treated as a melt of metal oxides) and the surrounding vapour phase, and the loss rate of each element is determined assuming Langmuir evaporation. These assumptions are based on the timescales for evaporation of the different elements being longer than for diffusion and heat transfer within the particle, as discussed in Vondrak et al. (2008). CABMOD also assumes that the meteoroid composition is that of ordinary chondrites (rather than, for example, carbonaceous chondrites). Despite these assumptions, the quantitative predictions of differential ablation rates by CABMOD were shown to agree well with time-resolved meteor head echoes measured by the Arecibo radar (Janches et al., 2009). The most volatile elements (Na and K) ablate first during atmospheric entry. Penetration deeper into the atmosphere raises the temperature to the point (> 1600^{o}C) at which the major constituents Fe, Mg and Si start to ablate. Finally, the most refractory major constituents (Ca, Ti) ablate if the particle temperature exceeds 2200^{o}C. At velocities greater than 50 km/s, CABMOD predicts complete ablation for meteoroids larger than 40 μm diameter (0.1 μg) at zenith angles between 0 and 85^{o}. However, at lower velocities ablation is dependent on mass and entry angle to the zenith (Vondrak et al., 2008). **Fig. 13** shows the threshold velocity at an entry angle of 40^{o} for ablation to commence, and the velocity for complete ablation to occur, in the case of

Ca, Mg and Fe. For instance, the model predicts that micrometeoroids having a mass 50 μg (diameter ~300 μm) have ablation threshold velocities for Ca, Mg, and Fe of ~15, 10, and 10 km/s, and complete ablation takes place at >30, 20, and 15 km/s, respectively (the minimum entry velocity, for a prograde orbit, is 11.2 km/s). For smaller meteoroid masses, both the threshold and complete ablation velocities are higher.

Molten meteoroids which reach the liquidus temperature of ~1700^{o}C form a Fe (or Ni) bead, or experience vaporization of Fe from the silicate melt causing a drastic change in chemical composition, including an enrichment of more refractory components such as CaO and Al_2O_3 (Hashimoto, 1983), and an increased weight percent of SiO_2 and MgO. A glass spherule will form if the entry conditions lead to the vaporization of Fe, but not SiO_2, MgO, or CaO. The entry velocity required to form glass spherules with diameters between 300 and 800 μm then lies between 20 and 15 km/s. The initial olivine composition of a meteoroid before entry into the atmosphere will start to deviate towards pyroxene stoichiometry due to evaporation of FeO. Any further heating will lead to evaporation of more refractory components such as SiO/SiO_2, rather than MgO which forms forsterite (Hashimoto, 1983). This stage is not reached in the case of glass spherules. Nevertheless, high enough temperatures are reached in the formation of glass spherules so that volatile elements such as Na and K completely ablate, and are below the detection limit. The major and trace elemental ratios can be used to understand volatile loss and peak temperatures experienced with respect to a chondritic precursor. The Mg/Si, Al/Si, Ca/Si and Fe/Si ratios are slightly depleted compared to those of CI chondrites (**Table 5**), and this indicates a small evaporative loss of Si from the bulk composition.

CABMOD is used to determine the entry conditions which will produce the required temperature (~1700^{o}C) and estimated mass loss (~20%) to form a glass spherule. Taking the case of a ~300 μm diameter meteoroid, entry at a large zenith angle (80–90^{o}) will require a velocity > 30 km/s, as shown in **Fig. 14**. At smaller zenith angles, lower velocities are required. For instance, a mass loss greater than 90% will be produced by a velocity and zenith angle in the range of 20–30 km/s and 0–80^{o}, respectively. For velocity of 16 km/s, the mass loss is greater than 90% for zenith angles between 0 and 40^{o} (**Fig. 14)**. At the minimum entry velocity of ~11 km/s, the upper limit of 16% ablation (even for entry zenith angle = 0^{o}) means that it is possible to produce a glass spherule. Since glass spherules are not expected to have experienced a mass loss during ablation that is greater than 20% (refer section 4.1), the CABMOD shows that the entry velocity should be restricted to 11–16 km/s, depending on zenith angle. Formation of glass spherules with much larger diameters and correspondingly much larger mass loss fractions seems unlikely, as larger size would probably lead

to fragmentation, and more prolonged heating will change the chemical composition, eventually forming a CAT spherule (Taylor et al., 2000).

4.3. Glass caps and pyroxene crystals in spherules

Glass caps have been observed on chondrules and the Fe and Si enrichment in the rims was suggested to be due to low temperature condensates (Alexander, 1995). These types of Si-rich caps are also found in chondrules of type I, but not in type II CR chondrites (Tissandier et al., 2002; Krot et al., 2004). A Si-rich cap may also be due to reduction of ferrous olivine (Jones and Danielson, 1997). This type of rim formation in micrometeorites may be analogous to that in chondrules. The rim thickness does not correlate strongly with the spherule diameter, as found in CM chondrites (Metzler et al., 1992) and unequilibrated ordinary chondrites (Huang et al., 1993). The relative composition of the spherule and the glass cap (~1–5 μm thickness) indicates significant fractionation of Si during atmospheric entry.

Genge (2006) observed several micrometeorites which developed igneous rims during atmospheric entry. These rims, in contrast to the present study, had compositions that were similar to those of the unmelted cores except for the loss by volatile elements. Large thermal gradients between the cores and rims of the micrometeorites suggested that this phenomenon was surficial to the micrometeorites (Genge, 2006). Further, the rims were vesicular, containing olivine microphenocrysts in a glassy mesostasis with the presence of magnetite. This also contrasts with the igneous rims in the present study which are all glassy and amorphous. The production of an igneous rim is due to the burning of a hydrous fine-grained matrix during entry, which is well supported by ablation experiments and models (Toppani et al., 2001; Szydlik and Flynn, 1992). Essentially, the igneous rims identified by Genge (2006) appear to be a low temperature phenomenon as they consists of scoriaceous cores which contain sulphide phases and void spaces, inhomogeneous rims that contain microporphyritic olivine in a matrix of glass and magnetites and void spaces in the rims. Based on experimental evidences by other investigators (e.g., Toppani and Libourel, 2002), Genge (2006) suggests a temperature of $\leq 1200^0$C for the formation of the igneous rims. However, he reports that in addition to olivine there is the presence of low Ca-pyroxene crystals (>10 μm size), which are considered primary rather than an atmospheric entry phenomenon. Chemically, however, they are highly dissimilar to those in the present study with very low silica contents and relatively higher Fe contents. More importantly, it was considered that the formation of pyroxene within the short periods of pulse heating would be difficult to achieve (Genge, 2006). The major conclusion of investigations made by Genge (2006) is that igneous rims on cgMMs (coarse-grained micrometeorites) are formed by melting of fine-grained matrix that is in contact with the surface of

the particle during atmospheric entry. This contrasts with the observations in the present study which indicate that the rims may have formed due to heating, chemical fractionation and centrifugal forces from a body which has undergone severe heating and homogenization (shown by the consistent loss of volatiles such as Fe, S, Na, K etc. as demonstrated for glass spherules by Taylor et al. (2000)).

Toppani and Libourel (2003) carried out pulse heating experiments on 200–400 μm fragments of the Orgueil (CI) and Murchison (CM2) chondrites under different oxygen fugacities in the temperature range of ~500–1500^{o}C over different time spans ranging from 5 to 120 seconds. Low temperature heating (i.e., below 1000^{o}C) did not yield major textural changes. In contrast, major changes such as recrystallization, zoning, and complete melting were observed at temperatures >1200^{o}C. However, over the range of temperatures and heating times employed, different varieties of spinel were produced and the material appeared not to homogenize; i.e., a fully homogenized glass spherule was not produced. Therefore, it is assumed here that the temperatures under which a glass spherule forms must be >1600^{o}C, where full homogenization of the composition takes place. Furthermore, pulse heating experiments by Greshake et al. (1998) showed an increase of olivine and pyroxene crystal size with increasing temperature. Nevertheless, steady-state evaporation experiments of chondritic melts at temperature in the range 700–2000^{0}C revealed pyroxene normative melts due to Fe loss accompanied by mass loss in excess of ~30%. Pyroxene normative melts quenched from high temperatures (as envisaged for the formation of cosmic spherules) formed glass rather than crystals (Hewins, 1983), although composition was sensitive to cooling rate; a higher content of Si crystals was seen to facilitate nucleation and growth of pyroxene crystals even at faster cooling rates. The crystalline grains in spherules AAS-62-54-#1-P1 and AAS-62-54#2-P27 are Mg-rich (~26-33wt%) and low-Ca (~1–4wt%) with compositions similar to the bulk. To have a homogenous chemical composition, the spherule must have been heated above the liquidus temperature. However, undercooling is required for the survival of the embryos (Connolly et al., 1998) that will be centres for the formation of pyroxene crystals (Radomsky and Hewins, 1990). The temperature must be just sufficient for rapid melting of small grain sizes (<60 μm), in contrast to larger grain sizes of 60–250μm (Connolly et al., 1998). This type of crystal growth is observed in some of the spherules (**Fig. 4**), and therefore has relevance for understanding nucleation and growth of crystals in chondrules. The majority of spherules are superheated droplets where complete dissolution of olivine has taken place with no nuclei available for the crystal to grow (Radomsky and Hewins, 1990; Connolly et al., 1998). This is supported by rapid cooling rates when compared to

barred or porphyritic textures. However, it is also possible that large sized crystals are preserved during atmospheric heating due to rapid cooling (Connolly et al., 1998).

4.4. Potential parent bodies of glass spherules

Major and trace element abundances show a considerable scatter, but indicate that a majority of the spherules have a broadly chondritic composition. The elemental ratios of Mg/Si, Al/Si, Ca/Si broadly correlate with carbonaceous chondrites as the possible parent bodies. The Fe/Si ratio in the spherules is depleted due to the evaporative loss of Fe during atmospheric entry (**Table 5**). The trace elements are enriched relative to CI chondrites. The average trace element compositions of 13 spherules normalized to CI, for the elements Zr, Hf, Y, Lu, Er, Ho, Tb, Tm, Dy, Gd, Nd, Sm, Pr, La, Yb, Ce, Eu and Sr, fall within the range ~1.5–1.8 × CI, thus having a close resemblance to carbonaceous chondrites (Lodders and Fegley, 1998). Whereas, three spherules (AAS-38-139-1-P12, AAS-38-77-P, AAS-38-164-P6) form an exception. The ~20% ablation when forming the glass spherules has not resulted in substantial divergence of trace element chemistry, except for few element. The REE (rare earth elements) of chondrites and the average of the spherules normalized to CI have a pattern that has close similarity to carbonaceous chondrites (CI, CO, CM, CV) (**Fig. 15**) (Brownlee et al., 1997, Herzog et al., 1999, Engrand et al., 2005, Yada et al., 2005). Previous work has proposed HED-like parent bodies for ~0.5% of micrometeorites forming glass spherules (Taylor et al., 2007; Cordier et al., 2011a). Therefore, the possibility of multiple precursors for glass spherules cannot be ruled out.

5. CONCLUSIONS

Investigations of 36 glass spherules retrieved from deep-sea sediments show that some of the larger spherules contained pyroxene normative grains. These large spherules (>300 μm) are likely to undergo fragmentation during the atmospheric entry to form two average sized spherules, thus enhancing the total percentage of glass spherules in unbiased collections. The fragmented bodies have different textures due to slight differences in the cooling rates. The spherule AAS-38-175-II-P2 shows the presence of a ~3 μm size platinum group nugget containing all six PGE, including the most volatile Pd, suggesting that the temperature experienced was not high enough to cause substantial ablation of Pd (~1700^0C). Aspects of the PGE nugget indicate that overall mass loss from the glass spherule was ~20%. The nugget could have formed during atmospheric entry due to segregation from a parent body of carbonaceous chondritic composition, or alternatively as a relict inclusion from CAI. Support for the latter comes from its inhomogeneous PGE composition and from similar elemental ratios of Os/Ir, Ru/Ir, Rh/Ir, and Pt/Rh.

The chemical ablation model (CABMOD) used in this study predicts that glass spherules with diameters >300 μm experience temperatures of ~1700^{o}C if their entry velocities are between 11 and 16 km/s. This temperature is sufficient to generate some evaporative loss of FeO, but largely retains SiO_2, MgO, and CaO in the particle, thus just effecting the change from an olivine normative composition to that of a pyroxene. The major, minor and trace element chemistry for the majority of the spherules supports carbonaceous (CI, CO, CM, CV) chondrites as the parent body.

ACKNOWLEDGEMENTS

NGR and MSP thank the Director of National Institute of Oceanography, Goa, for support. The assistance of Vijay Khedekar for SEM and EPMA (NIO) and Dipak Panda for EPMA (PRL) is gratefully acknowledged. We are grateful to an anonymous reviewer, as well as to G. Briani and C. Engrand for their methodical reviews that led to substantial improvement of the manuscript. This work is supported by Physical Research Laboratory, Ahmedabad, for the sanction of the PLANEX project (NGR and MSP). The modelling work at Leeds was supported by grant NE/G019487/1 from the UK Natural Environment Research Council. This is NIO's contribution No. xxxx.

REFERENCES

Alexander C. M. O'D. (1995) Trace element contents of chondrule rims and interchondrule matrix in ordinary chondrites. *Geochim. Cosmochim. Acta* **59**, 3247–3266.

Anders and Grevesse, (1989) Abundances of the elements - Meteoritic and solar. *Geochim. Cosmochim. Acta* **53**, 197–214.

Blanchard M. B., Brownlee D. E.,. Bunch T. E, Hodge P. W. and Kyte F. T. (1980) Meteoroid ablation spheres from deep-sea sediments. *Earth Planet. Sci. Lett.* **46**, 178–190.

Bland P. A., Smith T. B., Jull A. J. T., Berry F. J., Bevan A. W. R., Cloudt S. and Pillinger C. T. (1996) The flux of meteorites to the Earth over the last 50,000 years. *Mon. Not. R. Astron. Soc*. **283**, 551–565.

Bonte Ph., Jehanno C., Maurette M. and Brownlee D. E. (1987) Platinum metals and microstructure in magnetic deep sea cosmic spherules. *J. Geophy. Res.* **92**, 641–648.

Borisov A. and Palme H. (1995) The solubility of iridium in silicate melts: New data from experiments with $Ir_{10}Pt_{90}$ alloys. *Geochim. Cosmochim. Acta* **59**, 481–485.

Borisov A. and Palme H. (1997) Experimental determination of the solubility of platinum in silicate melts. *Geochim. Cosmochim. Acta* **61**, 4349–4357.

Borisov A., Palme H. and Spettel B. (1994) Solubility of Pd in silicate melts: Implications for core formation in the Earth. *Geochim. Cosmochim. Acta*, **58**, 705–716

Brenan J. M., McDonough W. F. and Ash R. (2005) An experimental study of the solubility and partitioning of iridium, osmium and gold between olivine and silicate melt. *Earth Planet. Sci. Lett.* **237**, 855–872.

Brenan J. M. and McDonough W. F. (2009) Core formation and metal–silicate fractionation of osmium and iridium from gold. *Nature Geoscience.* **2**, 798–801.

Brownlee D. E. and Bates B. (1983) Meteor ablation spherules as chondrule analogs. In: King, E.A. (Ed.), *Chondrules and their origins*. Lunar and Planetary Institute, Houston, pp. 10–25.

Brownlee D. E., Bates B. A. and Wheelock M. M. (1984) Extraterrestrial platinum group nuggets in deep-sea sediments. *Nature* **309**, 693–695.

Brownlee D. E. (1985) Cosmic Dust: Collection and Research. *Annu. Rev. Earth and Planet. Sci.* **13,** 147−173.

Brownlee D. E., Bates B. and Schramm L. (1997) The elemental composition of stony cosmic spherules. *Meteorit. Planet. Sci.* **32**, 157–175.

Campbell A. J. and Humayun M. (2005) Compositions of group IVB iron meteorites and their parent melt. *Geochim. Cosmochim. Acta* **69**, 4733–4744.

Ceplecha Z., BoroviËka J., Elford W. G., ReVelle D. O., Hawkes R. L., Porubcan V. and Šimek M. (1998) Meteor phenomena and bodies. *Space Sci. Rev.* **84**, 327–471.

Connolly H. C. Jr., Jones B. D. and Hewins R. H. (1998) The flash melting of chondrules: An experimental investigation into the melting history and physical nature of chondrule precursors. *Geochim. Cosmochim. Acta* **62**, 2725–2735.

Cordier C., Folco L. and Taylor S. (2011a) Vestoid cosmic spherules from the South Pole Water Well and Transantarctic Mountains (Antarctica): a major and trace element study. *Geochim. Cosmochim. Acta* **75**, 1199–1215.

Cordier C., Folco L., Suavet C., Sonzogni C. and Rochette P. (2011b) Major, trace element and oxygen isotope study of glass cosmic spherules of chondritic composition: The record of their source material and atmospheric entry heating. *Geochim. Cosmochim. Acta* **75**, 5203–5218.

Cordier C., van Ginneken M. and Folco L. (2011c) Nickel abundance in stony cosmic spherules: Constraining precursor material and formation mechanisms. *Meteoritics Planet. Sci.* **46**, 1110–1132.

Deer W.A., Howie R.A. and Zussman J. (1992) *An introduction to the Rock-forming Minerals* (2nd Edition). pp.696, Longman Scientific and Technical, New York.

Duprat J., Engrand C., Maurette M., Naulin F., Kurat G. and Gounelle M. (2006) The micrometeorite mass flux as recorded in Dome C central Antarctic surface snow. *Meteorit. Planet. Sci.* **41,** Suppl., A48.

Engrand C. and Maurette M. (1998) Carbonaceous micrometeorites from Antarctica. *Meteorit. Planet. Sci*. **33**, 565–580.

Engrand C., McKeegan K.D., Leshin L.A., Herzog G.F., Schnabel C., Nyquist L.E. and Brownlee D.E. (2005) Isotopic compositions of oxygen, iron, chromium, and nickel in cosmic spherules: Toward a better comprehension of atmospheric entry heating effects. *Geochim. Cosmochim. Acta* **69**, 5365–5385.

Ertel W., O'Neill H. St. C., Sylvester P. J. and Dingwell D. B. (1999) Solubilities of Pt and Rh in a haplobasaltic silicate melt at 1300°C. *Geochim. Cosmochim. Acta*, **63**, 2439–2449.

Genge M. J. and Grady M. M. (2002) The distribution of asteroids: Evidence from Antarctic micrometeorites. *Lunar Planet. Sci.* XXXIII, Lunar Planet. Inst., Houston. #1010 (abstr.).

Genge M. J. (2006) Igneous rims on micrometeorites. *Geochim. Cosmochim. Acta* **70**, 2603–2621.

Genge M.J., Engrand C., Gounelle M. and Taylor S. (2008) The classification of micrometeorites. *Meteorit. Planet. Sci.* **43**, 497–515.

Glass B.P., Mijenow D.w., Bohor B.F. and Meeker G.P. (1997) Fragmentation and hydration of tektites and microtektites. *Meteorit. Planet. Sci.* **32**, 333–341.

Glass B. P. and Koeberl C. (2006) Australasian microtektites and associated impact ejecta in the South China Sea and the Middle Pleistocene supereruption of Toba. *Meteorit. Planet. Sci.* **41**, 305–326.

Greshake A., Kloeck W., Arndt P., Maetz M., Flynn G. J., Bajt S. and Bischoff A. (1998) Heating experiments simulating atmospheric entry heating of micrometeorites: Clues to their parent body sources. *Meteorit. Planet. Sci*. **33,** 267–290.

Grossman L. and Ganapathy R. (1976) Trace elements in the Allende meteorite—II. Fine-grained, Ca-rich inclusions. *Geochim. Cosmochim. Acta* **40**, 967–977.

Harvey R.P. and Maurette M. (1991) The origin and significance of cosmic dust from the Walcott Névé, Antarctica. *In Proceedings of the 22nd Lunar and Planetary Science Conference*, *Houston, Texas*. Houston: Lunar and Planetary Institute, 21: 569– 578.

Hashimoto A. (1983) Evaporation metamorphism in the early solar nebula-evaporation experiments on the melt FeO-MgO–SiO_2-CaO-Al_2O_3. *Geochem. J.* **17**, 111–145.

Herzog G. F., Xue S., Hall G. S., Nyquist L. E., Shih C. Y., Wiesmann H. and Brownlee D. E. (1999) Isotopic and elemental composition of iron, nickel, and chromium in type I deep-sea spherules: implications for origin and composition of the parent micrometeoroids. *Geochim. Cosmochim. Acta* **63**, 1443–1457.

Hewins R H. (1983) Dynamic crystallization experiments as constraints on chondrule genesis. IN: Chondrules and their origins (A85-26528 11-91). Houston, TX, Lunar and Planetary Institute, 122–133.

Huang S., Benoit P. H. and Sears D. W. G. (1993) Metal and Sulfide in Semarkona Chondrules and Rims: Evidence for Reduction, Evaporation, and Recondensation During Chondrule Formation, *Meteoritics* **28**, 367.

Izett G. A. and Obradovich J. D. (1992) Laser-fusion $^{40}Ar/^{39}Ar$ ages of Australasian tektites. *Lunar Planet. Sci.* XXIII, Lunar and Planet. Inst., Houston. #1294 (abstr).

Janches D. and ReVelle D. O. (2005) Initial altitude of the micrometeor phenomenon: Comparison between Arecibo radar observations and theory, *J. Geophys. Res*. **110**, A08307, doi:10.1029/2005JA011022.

Janches, D., L. P. Dyrud, S. L. Broadley, and J. M. C. Plane (2009), First observation of micrometeoroid differential ablation in the atmosphere, *Geophysical Research Letters*, **36**, Article Number: L06101.

Jarosewich E., Nelen J. A. and Norberg J. A. (1980) Reference Samples for Electron Microprobe Analysis, *Geostand. Newslett.* **4**, 43–47.

Jones R. H. and Danielson L. R. (1997) A chondrule origin for dusty relict olivine in unequilibrated chondrites. *Meteorit. Planet. Sci*. **32**, 753–760.

Kita N. T., Nagahara H., Togashi S. and Morishita Y. (2000) A short duration of chondrule formation in the solar nebula: evidence from ^{26}Al in Semarkona ferromagnesian chondrules. *Geochim. Cosmochim. Acta* **64**, 3913–3922.

Krot A. N., Keil K., Goodrich C. A., Scott E. R. D. and Weisberg M. K. (2003). *Classification of meteorites. In Meteorites, comets, and planets*, edited by Davis A. M. Treatise on geochemistry, vol. 1. Amsterdam: Elsevier Pergamon. pp. 83–128.

Krot A. N., Libourel G., Goodrich C. A. and Petaev M. I. (2004) Silica-rich igneous rims around magnesian chondrules in CR carbonaceous chondrites: Evidence for fractional condensation during chondrule formation. *Meteorit. Planet. Sci*. **39**, 1931–1955.

Kunz J., Bollinger K., Jessberger E. K. and Storzer D. (1995) Ages of Australasian tektites *Lunar Planet. Sci.* XXVI, Lunar and Planet. Inst., Houston. #1405 (abstr).

Kurat G., Koeberl C., Presper T., Brandstätter F. and Maurette M. (1994) Petrology and geochemistry of Antarctic micrometeorites. Geochim. Cosmochim. Acta 58, 3879–3904.

Lal D. and Jull A. J. T. (2002) Atmospheric cosmic dust fluxes in the size range10^{-4} to 10 centimeters. *The Astrophy. J.* **576**, 1090–1097.

Lodders K. and Fegley B. Jr. (1998) *The Planetary Scientist's Companion*. Oxford University Press, New York.

Love S. G. and Brownlee D. E. (1991) Heating and thermal transformation of micrometeoroids entering the Earth's atmosphere, *Icarus* **89**, 26–43.

Love S. G. and Brownlee D. E. (1993) A Direct Measurement of the Terrestrial Mass Accretion Rate of Cosmic Dust. *Science* **262**, 550–553.

MacPherson G. J. (2003) *Meteorites, Comets and Planets*, vol. 1 (ed. A. M. Davis) of Treatise on Geochemistry (eds. H. D. Holland and K. K. Turekian), Elsevier-Pergamon, Oxford, pp. 201–246.

Maurette M., Hammer C., Brownlee D. E., Reeh N. and Thomsen H.H. (1986) Placers of Cosmic Dust in the Blue Ice Lakes of Greenland. *Science* **233**, 869-872.

Maurette M., Olinger C., Christophe Michel-Levy M., Kurat G, Pourchet M., Brandstatter F. and Bourot-Denise M. (1991) A collection of diverse micrometeorites recovered from 100 tonnes of Antarctic blue ice. *Nature* **351**, 44–47.

Metzler K., Bischoff A. and Stoeffler D. (1992) Accretionary dust mantles in CM chondrites: Evidence for solar nebula processes. *Geochim. Cosmochim. Acta* **56**, 2873–2897.

O'Neill H. St. C, Dingwell D. B, Borisov A, Spettel B. and Palme H. (1995) Experimental petrochemistry of some highly siderophile elements at high temperatures, and some implications for core formation and the mantle's early history. *Chem. Geol.* **120**, 255–273.

Palme H. and Wlotzka F. (1976) A metal particle from a Ca,Al-rich inclusion from the meteorite Allende, and the condensation of refractory siderophile elements. *Earth Planet. Sci. Lett.* **33,** 45-60.

Palme H. (2008) Platinum-group elements in cosmochemistry. *Elements* **4**, 233–238.

Pernicka E. and Wasson J. T. (1987) Ru, Re, Os, Pt and Au in iron meteorites. *Geochim. Cosmochim. Acta* **51**, 1717–1726.

Peucker-Ehrenbrink B. and Ravizza G. (2000). The effects of sampling artifacts on cosmic dust flux estimates: a reevaluation of nonvolatile tracers (Os, Ir). *Geochim. Cosmochim. Acta* **64**, 1965–1970.

Pouchou J. L. and Pichoir F. (1991) Quantitative analysis of homogeneous or stratified microvolumes applying the model "PAP". *In Electron Probe Quantification* (eds. K. F. J. Heinrich and D. E. Newbury). Plenum Press, New York, pp. 31–75.

Prasad M. S., Mahale V. P., and Kodagali V. N. (2007) New sites of Australasian microtektites in the Central Indian Ocean: Implications for the location and size of source crater. *J. Geophys. Res.* **112**, E06007, doi: 10.1029/2006JEO00857.

Radomsky P. M. and Hewins R. H. (1990). Formation conditions of pyroxene-olivine and magnesian olivine chondrules. *Geochim. Cosmochim. Acta,* **54**, 3537–3558.

Rubin A. E. and Grossman J. N. (2010) Meteorite and meteoroid: new comprehensive definitions. *Meteorit. Planet. Sci*. **45**, 114– 122.

Rudraswami N. G., Goswami J. N., Chattopadhyay B., Sengupta S. K. and Thapliyal A. P. (2008) ^{26}Al records in chondrules from unequilibrated ordinary chondrites: II. Duration of chondrule formation and parent body thermal metamorphism. *Earth Planet. Sci. Lett.* **274**, 93−102.

Rudraswami N. G., Parashar K. and Shyam Prasad M. (2011) Micrometer and nanometer size platinum group nuggets in micrometeorites from the deep sea sediments of Indian Ocean. *Meteorit. Planet. Sci*. **46**, 470–491.

Russell S. S., Srinivasan G., Huss G. R., Wasserburg G. J., and MacPherson G. J. (1996) Evidence for widespread ^{26}Al in the solar nebula and constraints for nebula time scales. *Science* **273**, 757–762.

Szydlik, P. P. and Flynn G. J. (1992) The internal temperature profiles of large micrometeorites during atmospheric entry. *Meteoritics* **27**, 294 (abstr.).

Tagle R. and Berlin J. (2008) A database of chondrite analyses including platinum group elements, Ni, Co, Au, and Cr: Implications for the identification of chondritic projectiles. *Meteorit. Planet. Sci*. **43**, *541-559.*

Taylor S. and Brownlee D. E. (1991) Cosmic spherules in the geological record. *Meteoritics* **26**, 203–211.

Taylor S., Lever J. H. and Harvey R. P. (1998) Accretion rate of cosmic spherules measured at the South Pole. *Nature* **392**, 899–903.

Taylor S., Lever J., and Harvey R. (2000). Numbers, types and compositional distribution of an unbiased collection of cosmic spherules. *Meteorit. Planet. Sci*. **35**, 651–666.

Taylor S., Herzog G. F. and Delaney J. S. (2007) Crumbs from the crust of Vesta: Achondritic cosmic spherules from the South Pole water well. *Meteorit. Planet. Sci*. **42**, 223–233.

Taylor S., Matrajt G. and Guan Y. (2012) Fine-grained precursors dominate the micrometeorite flux. *Meteorit. Planet. Sci*. 47, 550–564.

Thorseth I. H. , Furnes H. and Tumyr O. (1991) A textural and chemical study of Icelandic palagonite of varied composition and its bearing on the mechanism of the glass-palagonite transformation. *Geochim. Cosmochim. Acta* **55**, 731-749.

Tissandier L., Libourel G. and Robert F. (2002) Gas–melt interactions and their bearings on chondrule formation. *Meteorit. Planet. Sci.* **37**, 1377–1389.

Toppani A., and Libourel G. (2002) Experimental study of micrometeorite vesiculation. *Lunar Planet. Sci.* XXXIII. Lunar and Planet. Inst., Houston. #1473 (abstr).

Toppani A., Libourel G., Engrand C. and Maurette M. (2001) Experimental simulation of atmospheric entry of micrometeorites. *Meteorit. Planet. Sci*. **36**, 1377–1396.

Toppani A., and Libourel G. (2003) Factors controlling compositions of cosmic spinels: Application to atmospheric entry conditions of meteoritic materials. *Geochim. Cosmochim. Acta* **67**, 4621–4638.

Vondrak T., Plane J. M. C., Broadley S. and Janches D. (2008) A chemical model of meteoric ablation. *Atmos. Chem. Phys.* **8**, 7015–7031.

Wasson J.T. and Kallemeyn G.W. (1988) Compositions of chondrites. *Philosophical Transactions Royal Society London* **A 325**, 535–544.

Yada T., Nakamura T., Takaoka N., Noguchi T., Terada K., Yano H., Nakazawa T. and Kojima H. (2004). The global accretion rate of extraterrestrial materials in the last glacial period estimated from the abundance of micrometeorites in Antarctic glacier ice. *Earth, Planets and Space* **56**, 67–79.

Yada T., Nakamura T., Noguchi T., Matsumoto N., Kusakabe M., Hiyagon H., Ushikubo T., Sugiura N., Kojima H., and Takaoka N. (2005) Oxygen isotopic and chemical compositions of cosmic spherules collected from the Antarctic ice sheet: Implications for their precursor. *Geochim. Cosmochim. Acta* **69**, 5789–5804.

Figure Captions

Fig. 1. SEM images of 'complete' and fragmented glass spherules. (a) AAS-38-178-#1-P8 has large vesicles having diameter of ~200 μm. (b–c) The fragmented ones have scalloped outlines and have grain boundaries in the interior. (d–e) They are scalloped and smooth interior. (f) AAS-38-176-II-P16 has a chromite gain and large vesicle presence. An arrow is pointed towards the chromite grain.

Fig. 2. Progressive stages in the fragmentation of glass spherules. (a–c) SEM images of large sized spherules that show no evidence of fragmentation. (d) Spherule with a Fe–Ni bead. (e–i) Development of a fissure which deepens progressively (the bottom half of spherule (Fig. 2i) a scalloped appearance probably due to degassing) enveloping the spherules partially.

Fig. 3. Presence of glass cap on spherules. (a) Polished section optical microscopic image of AAS-62-54-#1-P1 showing presence of glass cap. Pyroxene crystal development can be seen in the spherule, especially to the left side of the image. (b) Polished section optical microscopic image of AAS-62-54-#2-P27 having a glass cap with a scalloped appearance in the bottom half of the spherule. (c) SEM image of whole spherule AAS-38-186-P1 along with Fe–Ni bead. The spherule also has a glass cap covering the upper half of the spherule. The arrow indicate the glass cap on the spherule. (d) SEM image of unpolished spherule AAS-38-77-P3 showing presence of a Fe-Ni bead with a glass cap. The lower half of the spherule surface appears to have experienced degassing.

Fig. 4. Presence of pyroxene crystals inside the spherules AAS-62-54-#1-P1 and AAS-62-54-#2-P27. The parts of the spherules enclosing these crystals have glass caps (also see Fig. 2h and i)

Fig. 5. Platinum group nugget-bearing spherule. (a) BSE image of the whole spherule AAS-38-175-II-P2 is shown. Radial grooves are seen which are either flow lines or crystallization patterns. (b) Polished section of the spherule AAS-38-175-II-P2, with Platinum group element nugget at the edge of the spherule. The arrow marked seems to be breaking point for the formation of two spherule. The nugget is enclosed in marked circle. (c) Closer view of the platinum group element nugget that is at the edge of the spherule. (d) Enlarged observation shows that the nugget of ~3 μm is divided with some strip in between and has a surrounding thick ring. Marked regions 1 and 2 are analyzed using SEM–EDS, the data is provided in **Table 3**.

Fig. 6. Abundance of major elements in the spherules in comparison with chondrites. The data are normalized to CI chondrite compositions (Anders and Grevesse, 1989) and Si abundance. The elements are plotted in order of increasing volatility from left to right (except for Fe). Na is

completely depleted from all spherules. The data for spherules are shown in colors, while those for meteorites are in grey.

Fig. 7. Trace element composition of spherules normalized to CI chondrites (Lodders and Fegley, 1998). The elements are plotted in order of decreasing volatility from left to right. The thick grey line is the average of the 12 spherules.

Fig. 8. CI chondrite normalized PGE ratios compared with chondritic meteorites (grey coloured lines with different symbols are H, L LL, EH, and EL chondrites), one CAI from Allende (filled square) with spherule AAS-38-175-II-P2 nugget data (filled diamond). The nugget data in spherule seems to have similar trend as that of one CAI from Allende (CAI values from Palme and Wlotzka, 1976).

Fig. 9. The Os/Ir (normalized to CI) of chondrites (Tagle and Berlin, 2008) , one CAI from Allende (Palme and Wlotzka, 1976), iron meteorites (Pernicka and Wasson, 1987; Campbell and Humayun, 2005), and PGE nugget data from I-type spherules (Brownlee et al., 1984; Bonte et al.,1987; Rudraswami et al., 2011) along with the nugget from spherule AAS-38-175-II-P2.

Fig. 10. Fe/Mg verses Fe/Mn data for glass spherules from the present study. The dashed line is the spread in chondritic values. The filled circle are from the present study. The empty circle is spherule AAS-38-175-II-P2.

Fig. 11. Ca/Si (atom) verses Al/Si (atom) are plotted for all the glass spherules studied from deep sea sediments collection in Indian Ocean. The dark line is for the solar values. Hexagonal marked with a dot is the glass spherule AAS-38-175-II-P2 with platinum group nugget.

Fig. 12. Histogram plot of diameters (μm) of spherules in this study.

Fig. 13. The threshold velocity for ablation (dashed line) and the velocity at which complete ablation occurs (solid lines) for Fe, Mg, and Ca depend strongly on the meteoroid mass, both decreasing with increasing mass. The Chemical Ablation Model (CABMOD) (Vondrak et al. , 2008) was used to produce this result for entry zenith angle of 40.

Fig. 14. Percentage of mass ablated from a 300μm diameter micrometeoroid as a function of zenith angle and velocity, predicted by CABMOD (Vondrak et al, 2008).

Fig. 15. Comparison of averaged REE patterns of spherules and chondrites, data are normalized to CI chondrite composition (Lodders and Fegley, 1998).

Table 1. Averaged major elemental compositions (wt%) of the glass spherules obtained by defocused-beam electron microprobe analyses.

Sample	N	SiO_2	MgO	Al_2O_3	CaO	TiO_2	Cr_2O_3	MnO	FeO	NiO	Total
AAS38-178#2-P1	9	44.8	31.7	3.1	2.3	0.1	0.2	0.3	17.6	0.1	100.2
AAS-38-194#1-P4	4	43.0	33.2	3.0	2.1	0.1	–	0.3	20.5	0.5	102.7
AAS-38-139-#1-P12	6	44.6	27.0	2.9	2.4	0.1	0.3	0.3	22.5	0.1	100.1
AAS-38-139-#1-P39	7	40.8	29.0	3.7	3.4	0.1	–	0.3	23.3	–	100.7
AAS-38-178,#1-P8	11	47.7	26.6	3.6	2.4	0.1	0.1	0.3	20.0	0.1	101.8
AAS-38-178,#1-P12	8	46.7	29.7	2.7	1.0	0.2	0.4	0.4	20.9	–	102.0
AAS-38-178,#1-P14	9	44.9	28.9	2.0	1.2	0.1	0.3	0.3	24.5	–	102.4
AAS-62-54#1-P1	8	47.3	29.8	2.8	1.9	0.1	0.3	0.4	18.0	0.1	100.7
AAS-62-54-#2-P11	7	45.3	33.3	3.0	2.3	0.1	0.2	0.4	17.2	0.1	101.9
AAS-62-54-#2-P27	7	46.6	29.5	3.2	1.2	0.1	0.1	0.4	20.3	0.3	101.6
AAS-38-175-II-P2	10	44.0	30.3	3.3	2.7	0.2	0.2	0.5	17.8	0.2	99.1
AAS-38-77-P3	16	48.3	26.0	2.0	2.4	0.1	0.1	0.3	20.7	–	99.9
AAS-38-164-P6	15	49.2	30.6	2.5	1.8	0.1	0.2	0.4	15.7	0.1	100.5
AAS-38-147-I-P2	15	40.8	29.2	3.1	4.3	0.1	0.1	0.3	22.7	0.1	100.6
AAS-38-178-II-P14	20	46.6	32.1	2.4	1.9	0.1	0.2	0.4	16.1	0.2	99.9
AAS-38-178-II-P16	14	49.1	32.3	0.8	0.8	0.1	0.5	0.4	17.0	0.1	101.1
AAS-38-175-P23	10	44.7	31.1	2.3	3.6	0.1	0.2	0.3	17.2	–	99.5
AAS-38-175-P31	10	41.2	29.5	3.1	2.4	0.1	0.2	0.3	24.5	0.1	101.3
AAS-38-186-P17	10	46.0	28.9	2.8	2.3	0.1	0.3	0.4	18.8	0.3	99.8
AAS-38-186-P23	10	40.1	32.7	5.4	3.4	0.3	–	0.1	17.9	–	100.1

N is the number of analysis for which average is calculated. The electron microprobe analyses were performed with a 15 μm beam size, beam current of 12 nA and accelerating voltage of 15kV. The element such as S, P and K were measured, but have not been shown in the table as they are below the detection limit.

Table 2. Electron microprobe data (wt%) of mineral, chromite, silica cap in glass spherules.

Sample	Phase*	SiO_2	MgO	Al_2O_3	CaO	TiO_2	Cr_2O_3	MnO	FeO	NiO	Total
AAS-38-175-II-P2	Lpx	44.0	30.4	3.3	2.6	0.1	0.1	0.4	17.5	0.2	98.8
AAS-62-54-#1-P1	Lpx	48.4	30.5	2.8	1.8	0.1	0.4	0.3	17.9	0.1	102.4
AAS-62-54#2-P27	Lpx	46.3	28.5	3.2	0.9	0.1	0.2	0.4	12.9	7.1	99.7
AAS-38-178-II-P16	Chr	2.2	7.4	5.9	0.1	1.9	55.1	–	26.2	0.1	99.6

*Phase are as follows: Lpx is low-Ca pyroxene and Chr is chromite.

Table 3. EDS data (wt%) of micrometer-sized platinum group nugget found in glass spherule AAS-38-175-II-P2. The outer and inner half are marked as 1 and 2 in Figure 5.

Element	Outer half	Inner half
Fe	14.7	57.2
Ni	39.5	26.8
Ru	11.7	3.7
Rh	2.2	0.5
Pd	6.3	2.0
Os	4.0	1.9
Ir	7.2	3.6
Pt	14.4	4.4

Table 4. Elemental ratios of platinum group element in different chondrites, one CAI in the Allende chondrite and nugget of glass spherule.

	Os/Ir	Ru/Ir	Rh/Ir	Pt/Ir	Pd/Ir	Pt/Os	Pt/Rh	Pt/Ru	Pt/Pd	Ru/Os
CI	1.06	1.52	0.29	2.03	1.19	1.91	7.12	1.34	1.70	1.43
CO	1.08	1.49	–	1.66	0.94	1.54	–	1.12	1.76	1.38
CM	1.12	1.50	0.26	1.84	1.07	1.65	6.99	1.22	1.71	1.35
CV	1.06	1.52	0.28	1.90	0.93	1.79	6.89	1.26	2.04	1.43
CK	1.07	1.45	0.28	2.02	0.97	1.89	7.34	1.39	2.08	1.36
CR	1.05	1.49	–	1.94	1.18	1.84	–	1.30	1.65	1.41
CH	1.08	1.47	–	1.50	0.90	1.38	–	1.02	1.66	1.36
CB	1.09	1.42	0.34	1.80	1.01	1.66	5.39	1.27	1.78	1.31
K	1.07	1.53	–	–	–	–	–	–	–	1.43
R	1.06	1.48	–	–	–	–	–	–	–	1.39
H	1.07	1.51	0.31	2.08	1.10	1.94	6.78	1.37	1.89	1.41
L	1.07	1.49	0.33	2.05	1.22	1.91	6.21	1.38	1.68	1.39
LL	1.08	1.55	0.34	2.10	1.49	1.94	6.16	1.35	1.42	1.43
L/LL	1.12	1.51	–	1.94	1.45	1.73	–	1.28	1.34	1.35
EH	1.13	1.62	0.33	2.06	1.62	1.83	6.20	1.28	1.28	1.43
EL	1.11	1.53	0.33	2.01	1.31	1.81	6.16	1.32	1.54	1.38
CAI	0.55	1.02	0.34	2.43	–	4.46	7.13	2.38	–	1.88
Nugget	0.55	1.34	0.22	1.62	0.72	2.93	7.71	1.20	2.25	2.42

Data for chondrites are from Tagle and Berlin (2008) and data for the Allende CAI are from Palme and Wlotzka (1976).

Table 5. Different element ratios (atomic) of glass spherules (n=20) with chondrites composition (Wasson and Kallemeyn, 1988). The error given in the glassy spherules are one sigma standard deviation. The AAS-38-175-II-P2 is the spherule with platinum group nugget of ~3 μm. It is provided to have comparisons with various chondrite groups.

	Mg/Si	Al/Si	Ca/Si	Fe/Si	Ti/Si
Glassy (n=20)	0.997±0.100	0.075±0.027	0.057±0.026	0.363±0.067	0.002±0.001
AAS-38-175-II-P2	1.027	0.087	0.065	0.334	0.003
CI	1.068	0.085	0.061	0.872	0.002
CM	1.048	0.095	0.069	0.819	0.003
CO	1.054	0.094	0.070	0.784	0.003
CV	1.074	0.117	0.085	0.758	0.004
H	0.957	0.070	0.052	0.818	0.002
L	0.931	0.069	0.050	0.584	0.002
LL	0.935	0.066	0.048	0.492	0.002
EH	0.733	0.050	0.036	0.873	0.002
EL	0.876	0.059	0.038	0.595	0.002

Fig. 1

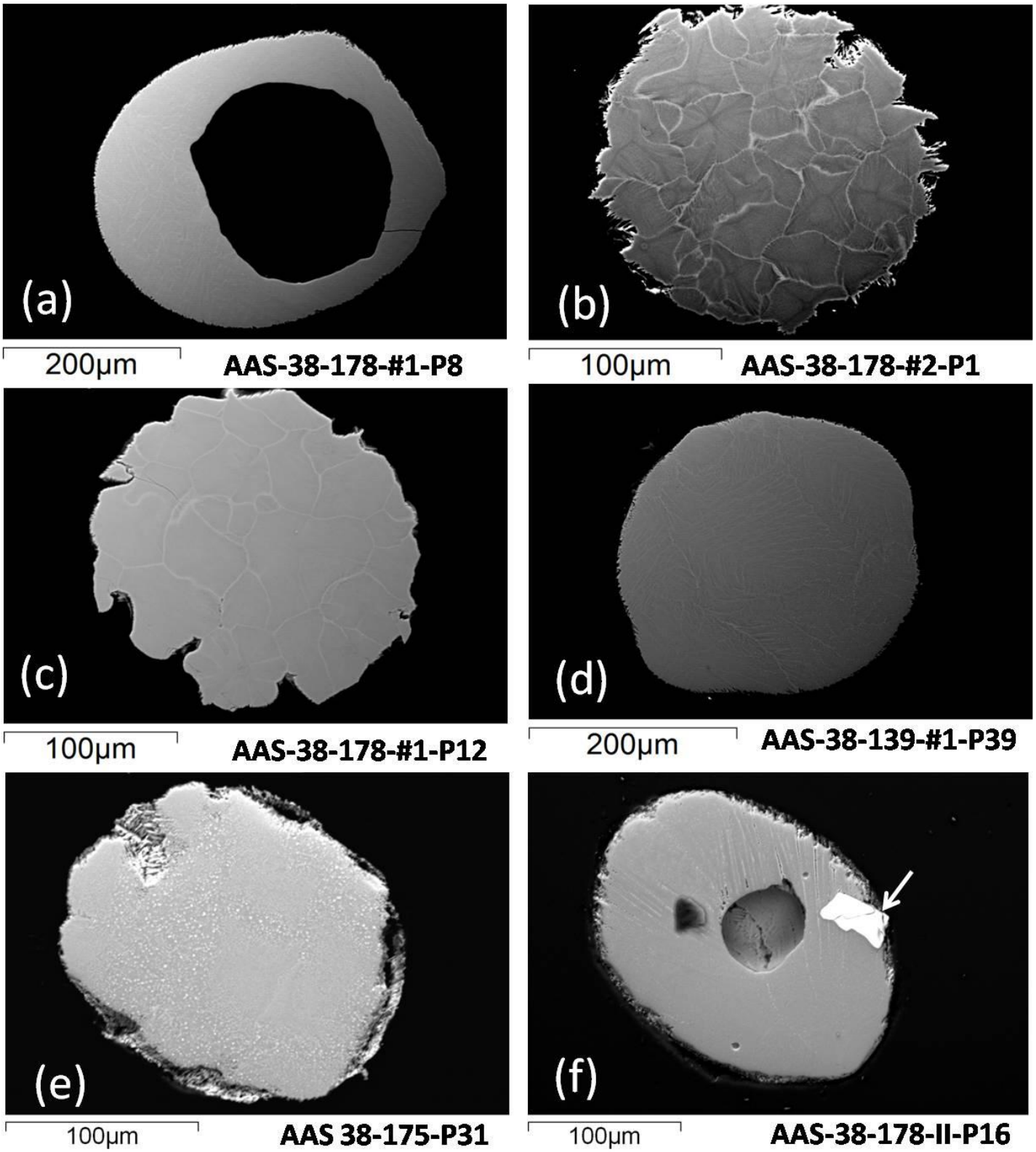
(a)
200µm
AAS-38-178-#1-P8
(b)
100µm
AAS-38-178-#2-P1
(c)
100µm
AAS-38-178-#1-P12
(d)
200µm
AAS-38-139-#1-P39
(e)
100µm
AAS 38-175-P31
(f)
100µm
AAS-38-178-II-P16

Fig. 2

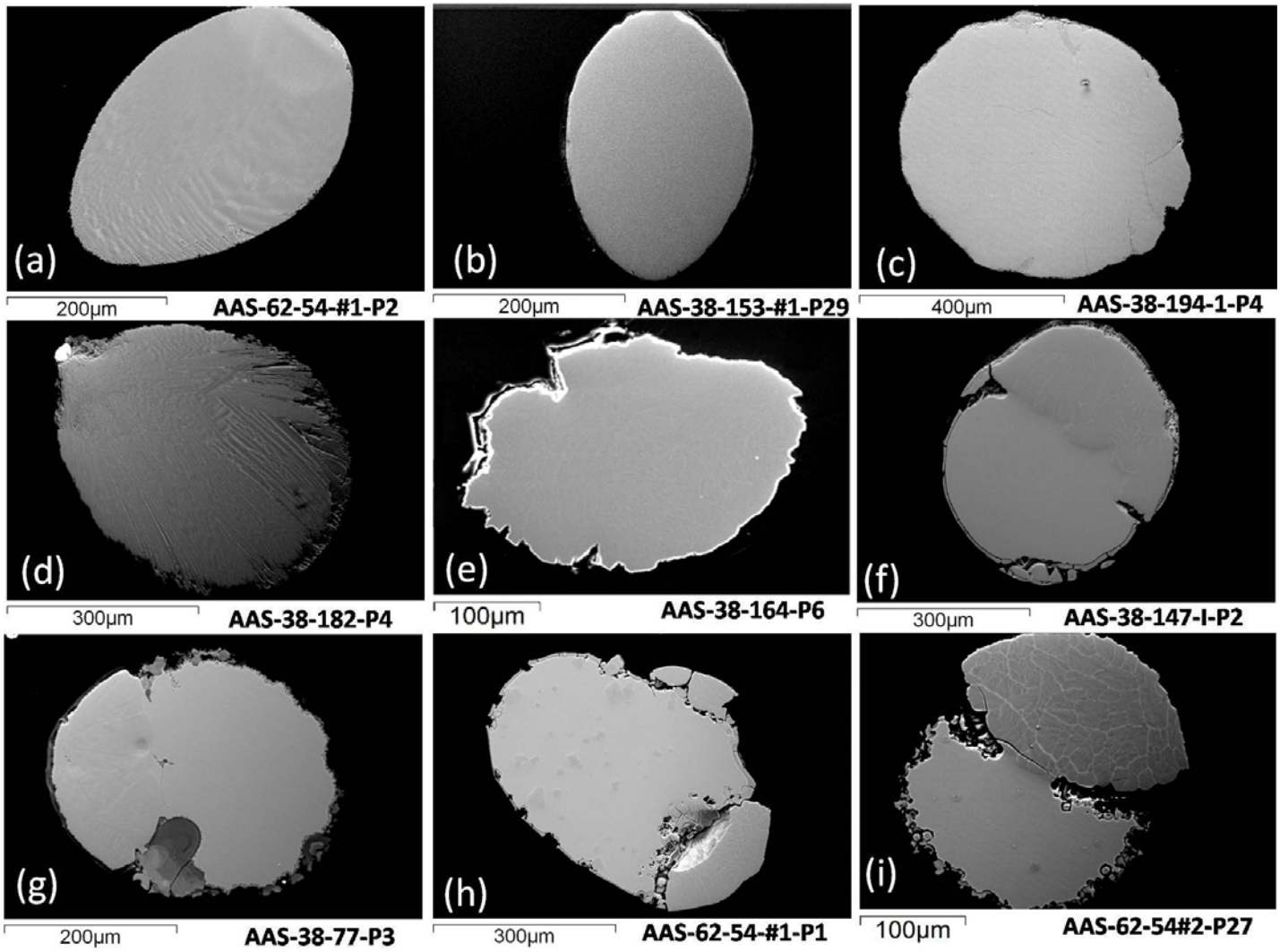
(a)
200μm
AAS-62-54-#1-P2
(b)
200μm
AAS-38-153-#1-P29
(c)
400μm
AAS-38-194-1-P4
(d)
300μm
AAS-38-182-P4
(e)
100μm
AAS-38-164-P6
(f)
300μm
AAS-38-147-I-P2
(g)
200μm
AAS-38-77-P3
(h)
300μm
AAS-62-54-#1-P1
(i)
100μm
AAS-62-54#2-P27

Fig. 3

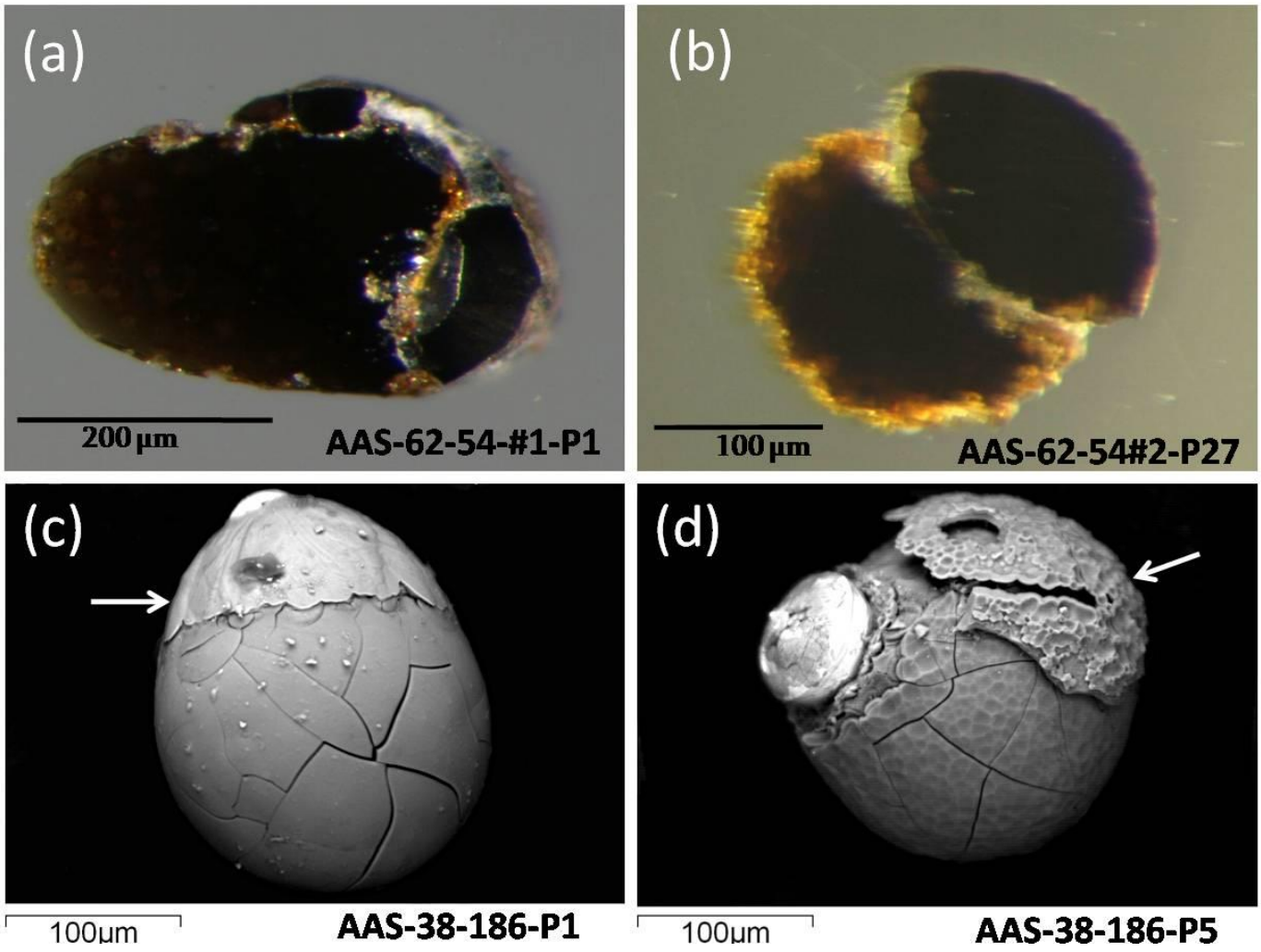
(a)
200 µm
AAS-62-54-#1-P1
(b)
100 µm
AAS-62-54#2-P27
(c)
100µm
AAS-38-186-P1
(d)
100µm
AAS-38-186-P5

Fig. 4

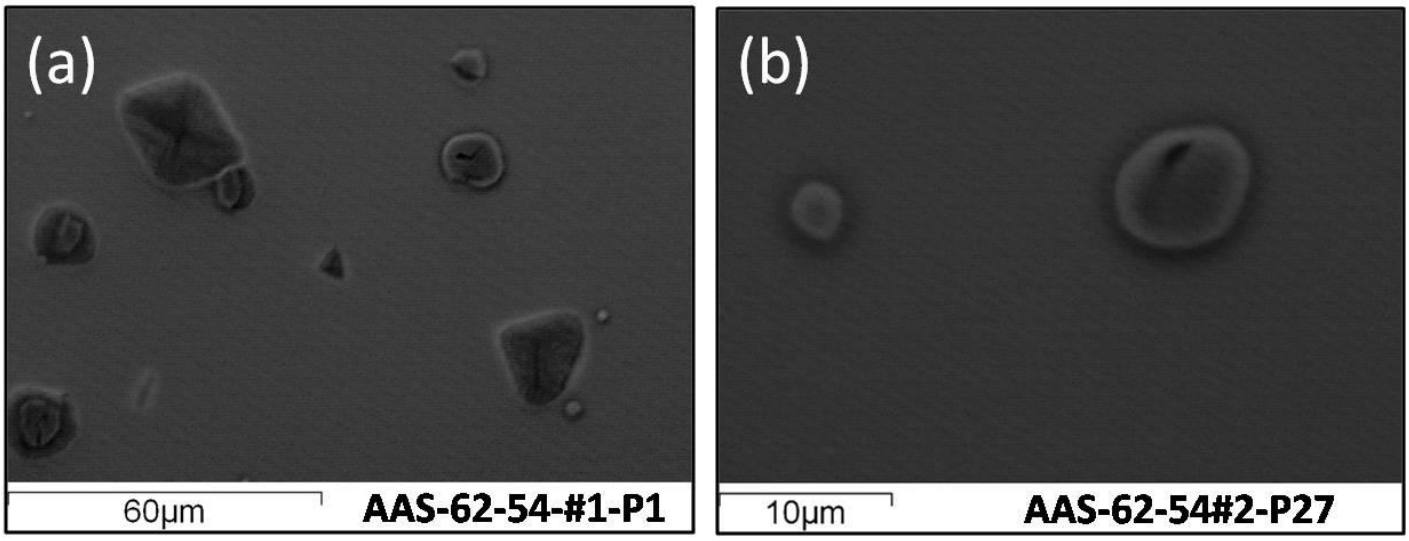

Fig. 5

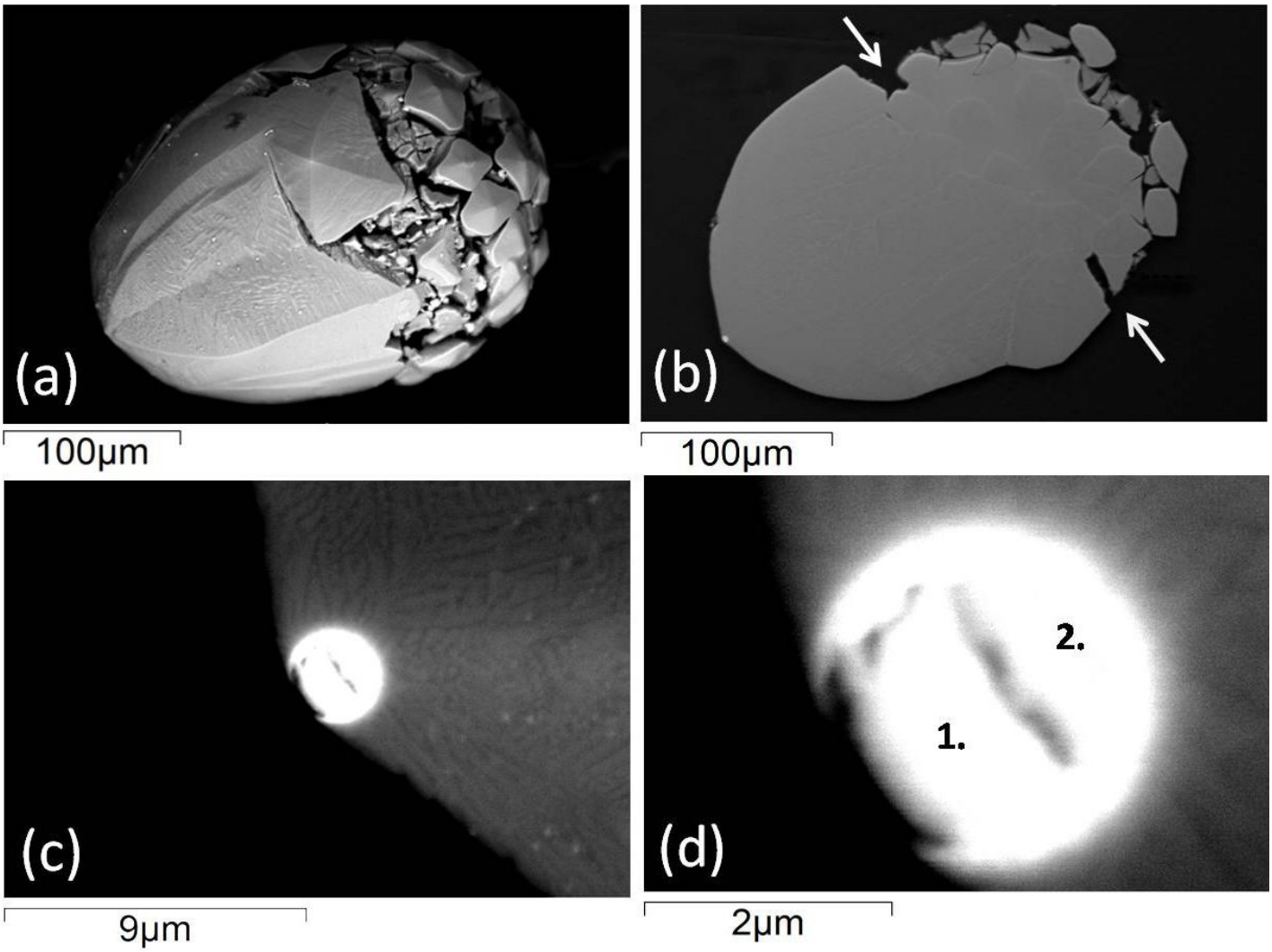

Fig. 6

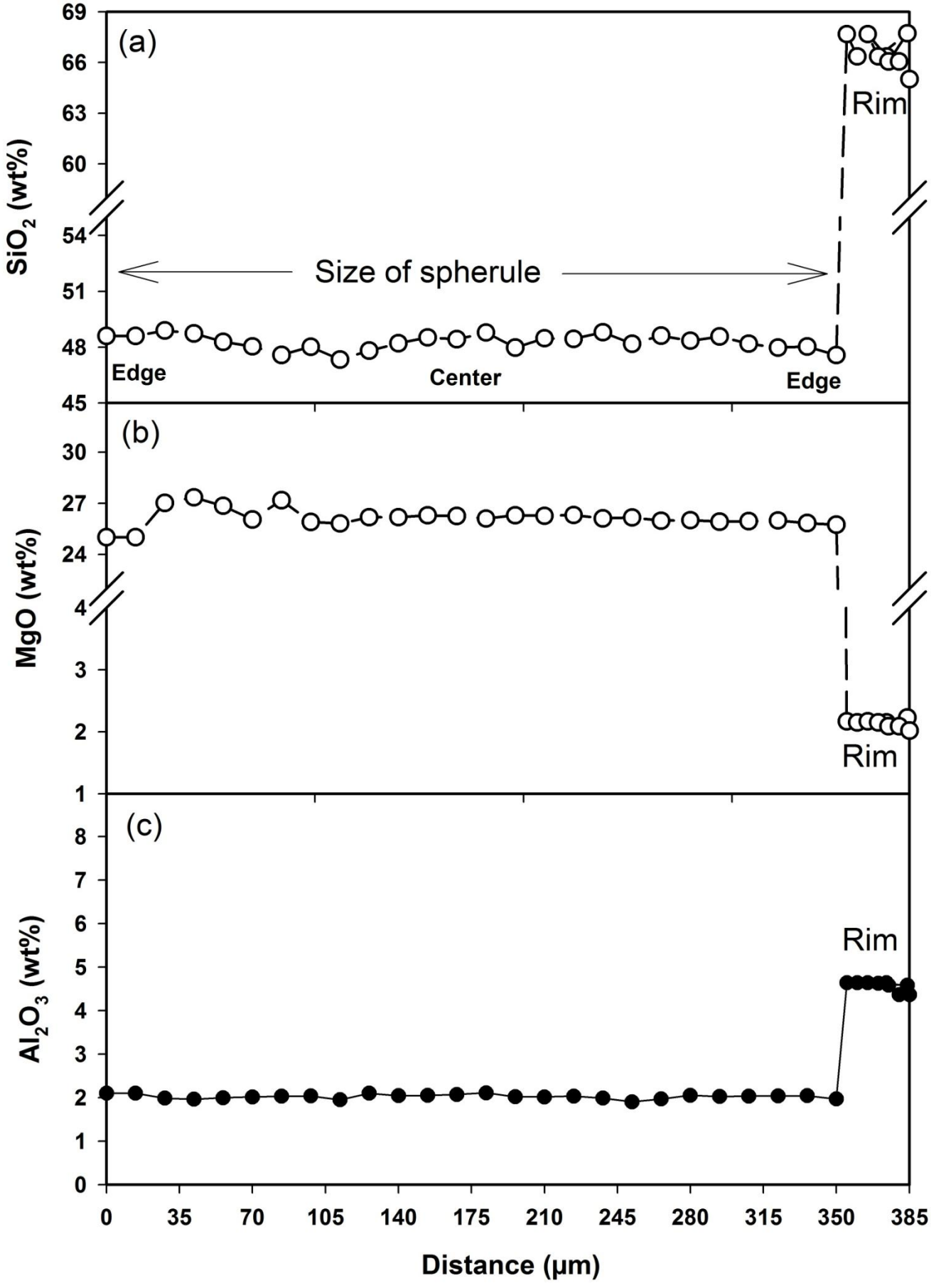
(a)
(b)
(c)
SiO_2 (wt%)
MgO (wt%)
Al_2O_3 (wt%)
Size of spherule
Edge
Center
Edge
Rim
Rim
Rim
Distance (μm)
0
35
70
105
140
175
210
245
280
315
350
385

Fig. 7

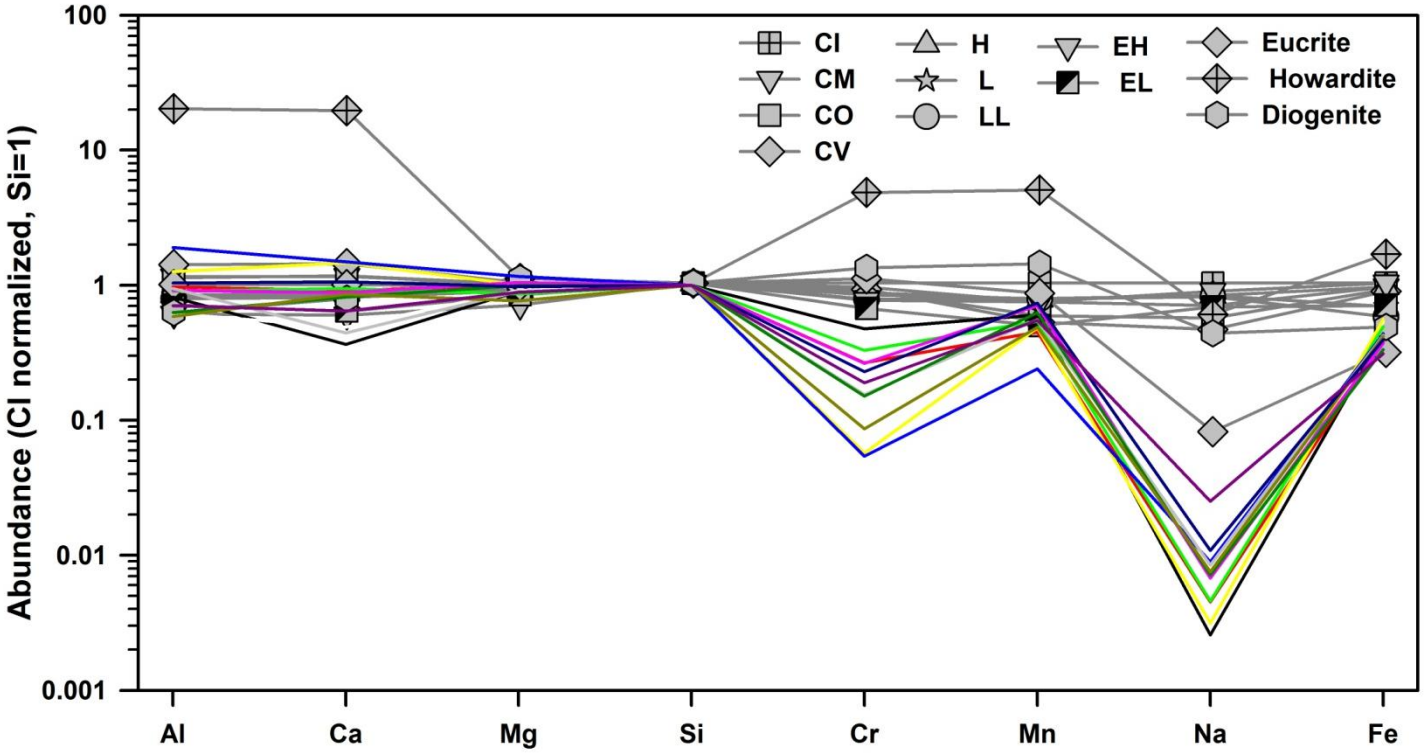
Abundance (CI normalized, Si=1)
100
10
1
0.1
0.01
0.001
Al
Ca
Mg
Si
Cr
Mn
Na
Fe
CI
CM
CO
CV
H
L
LL
EH
EL
Eucrite
Howardite
Diogenite

Fig. 8

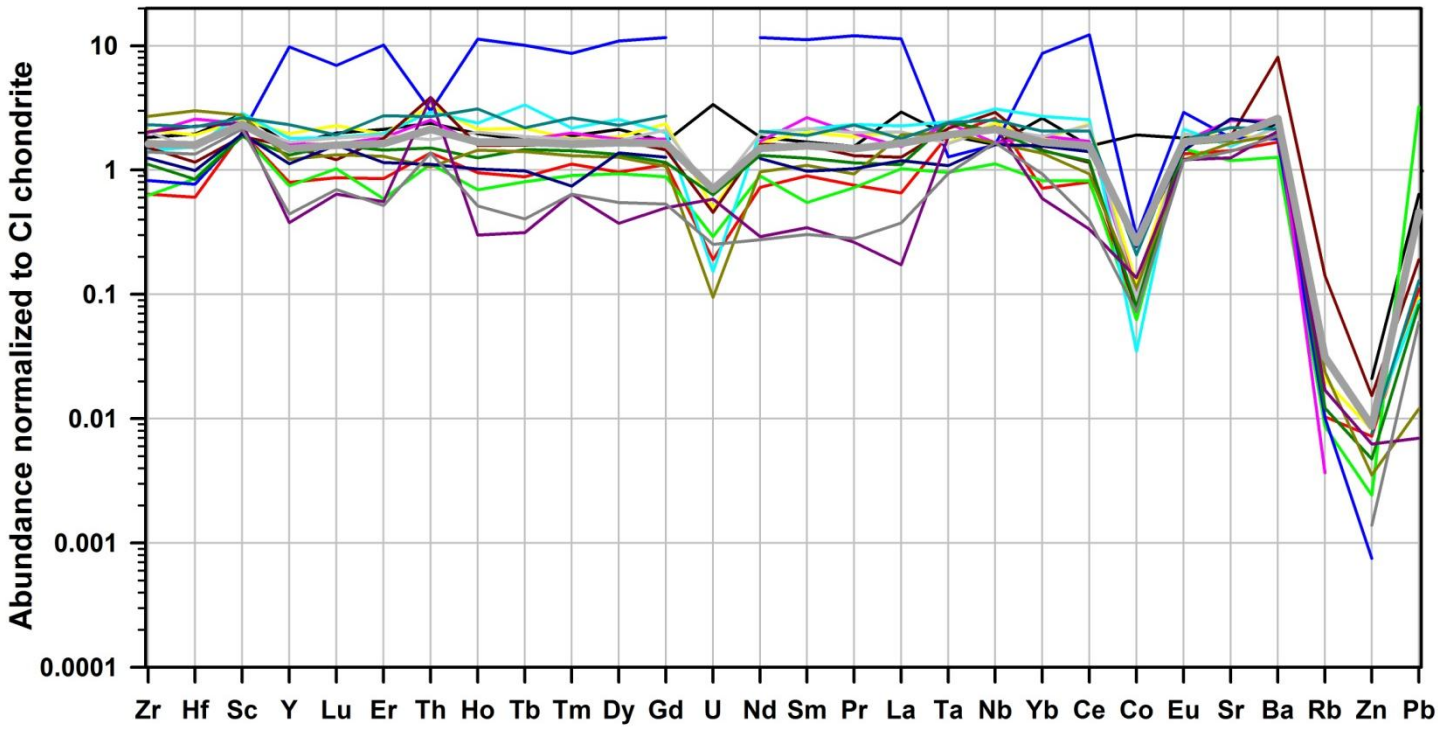
Abundance normalized to CI chondrite
10
1
0.1
0.01
0.001
0.0001
Zr Hf Sc Y Lu Er Th Ho Tb Tm Dy Gd U Nd Sm Pr La Ta Nb Yb Ce Co Eu Sr Ba Rb Zn Pb

Fig. 9

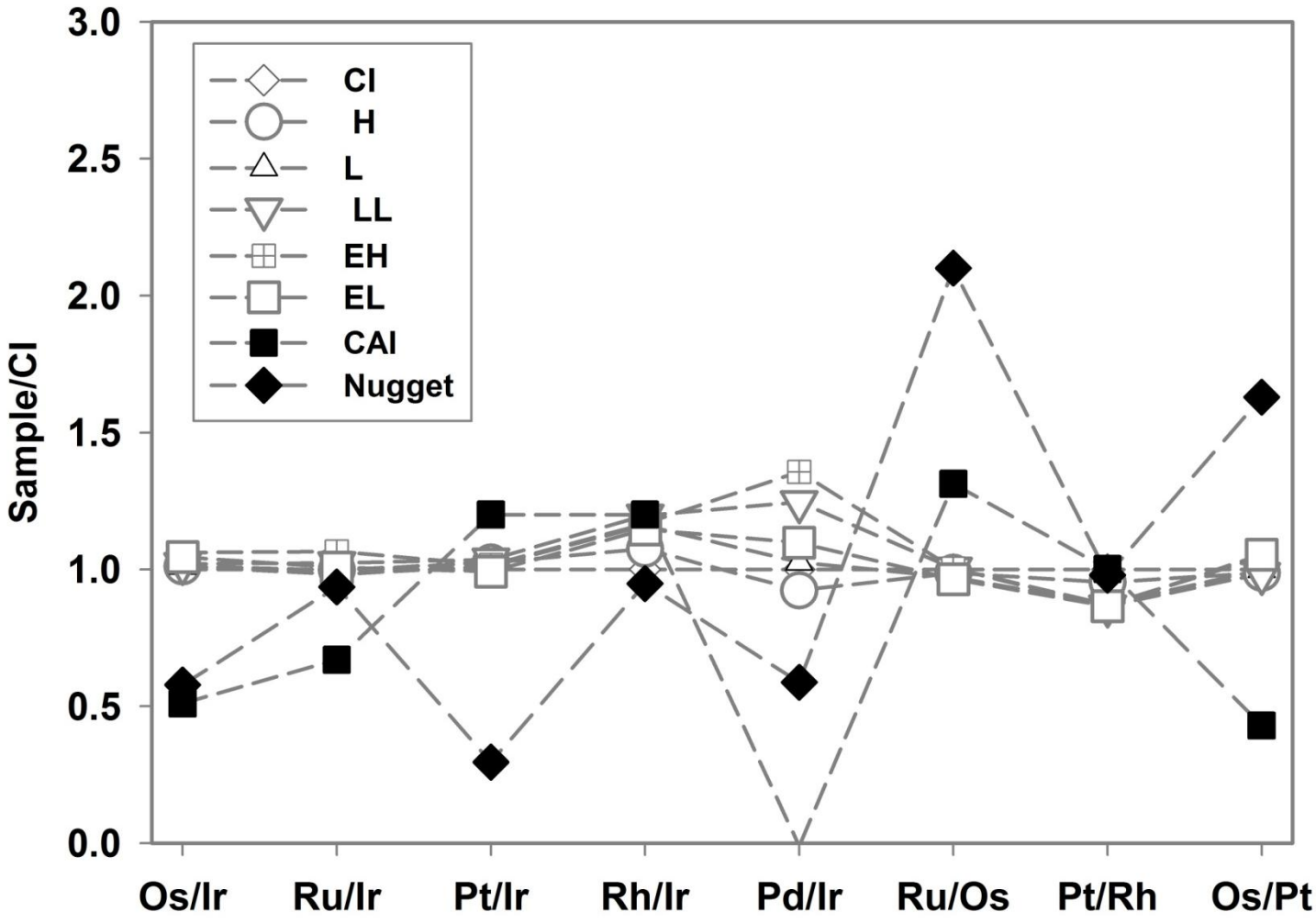
3.0
2.5
2.0
1.5
1.0
0.5
0.0
Sample/CI
CI
H
L
LL
EH
EL
CAI
Nugget
Os/Ir
Ru/Ir
Pt/Ir
Rh/Ir
Pd/Ir
Ru/Os
Pt/Rh
Os/Pt

Fig. 10

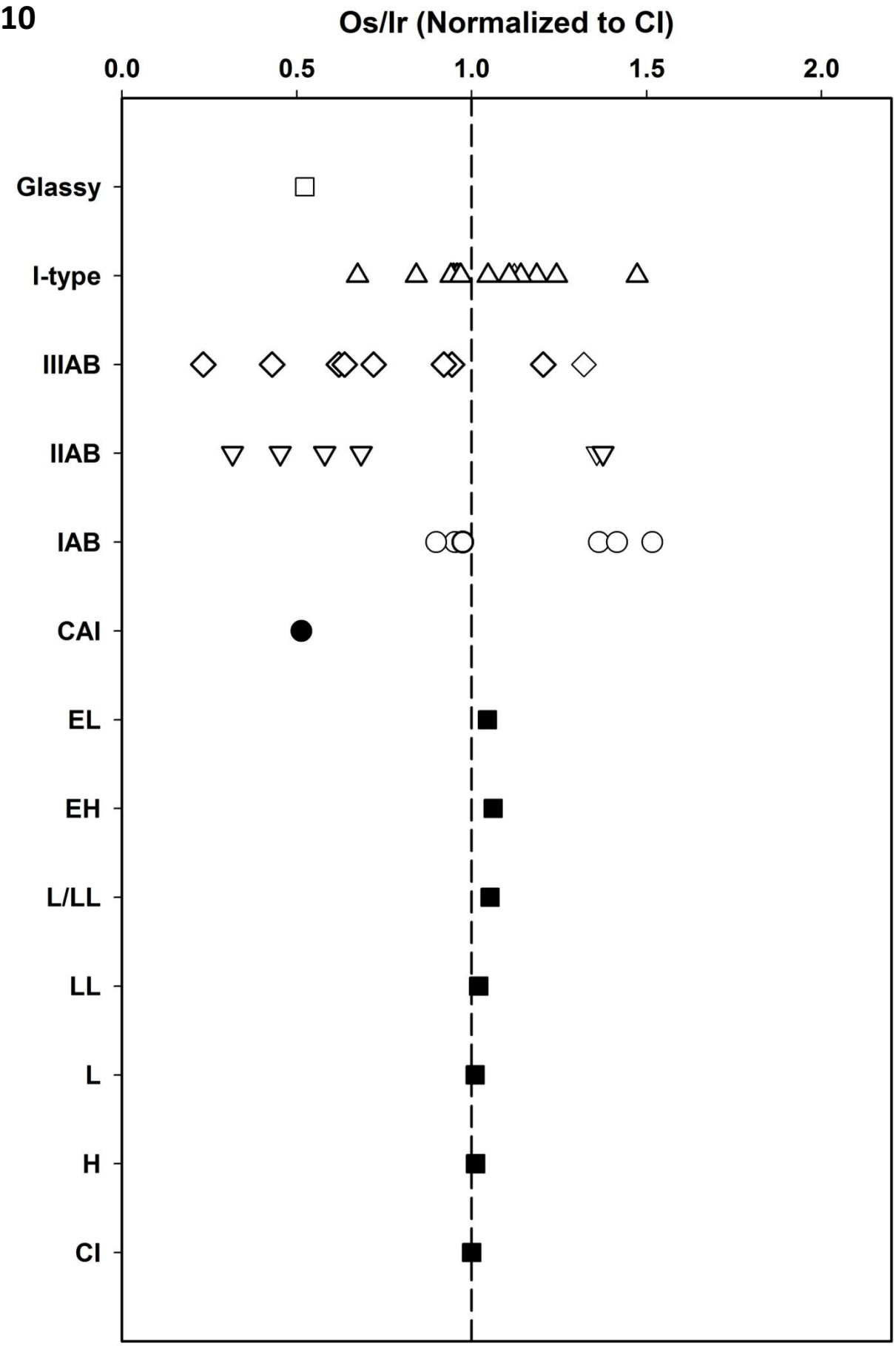
Os/Ir (Normalized to CI)
0.0
0.5
1.0
1.5
2.0
Glassy
I-type
IIIAB
IIAB
IAB
CAI
EL
EH
L/LL
LL
L
H
CI

Fig. 11

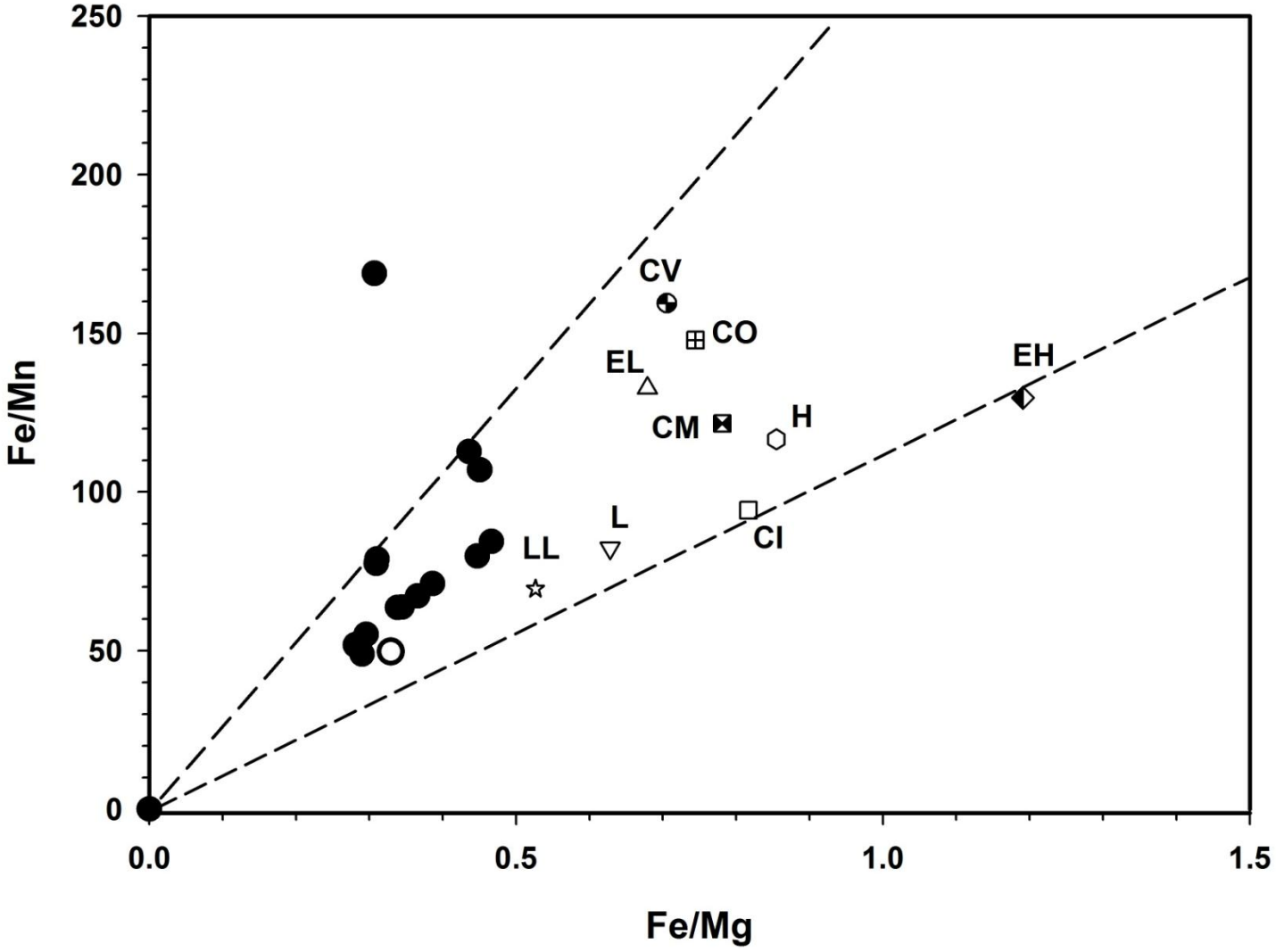

Fig. 12

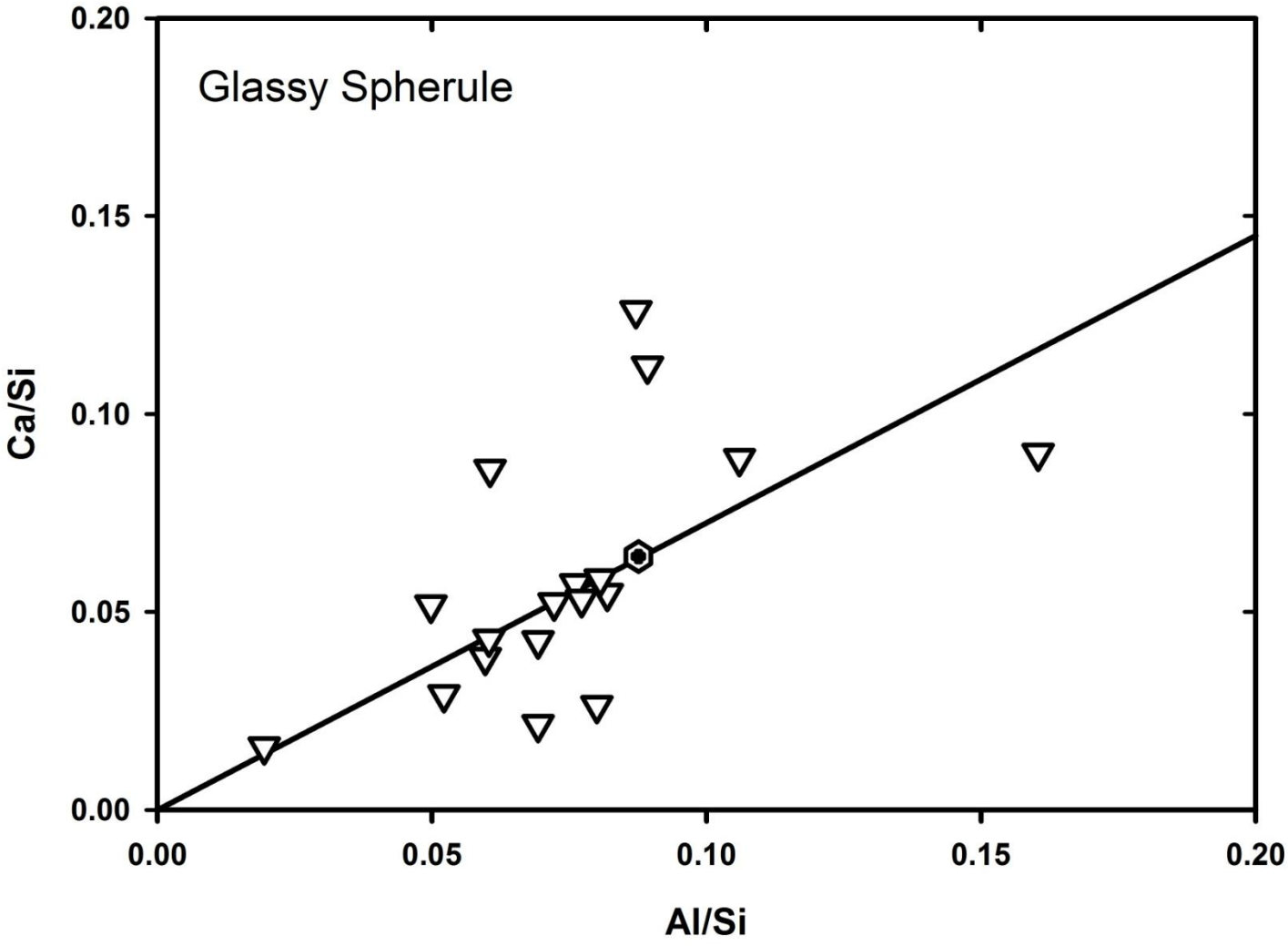
Glassy Spherule
0.20
0.15
0.10
0.05
0.00
Ca/Si
0.00
0.05
0.10
0.15
0.20
Al/Si

Fig. 13

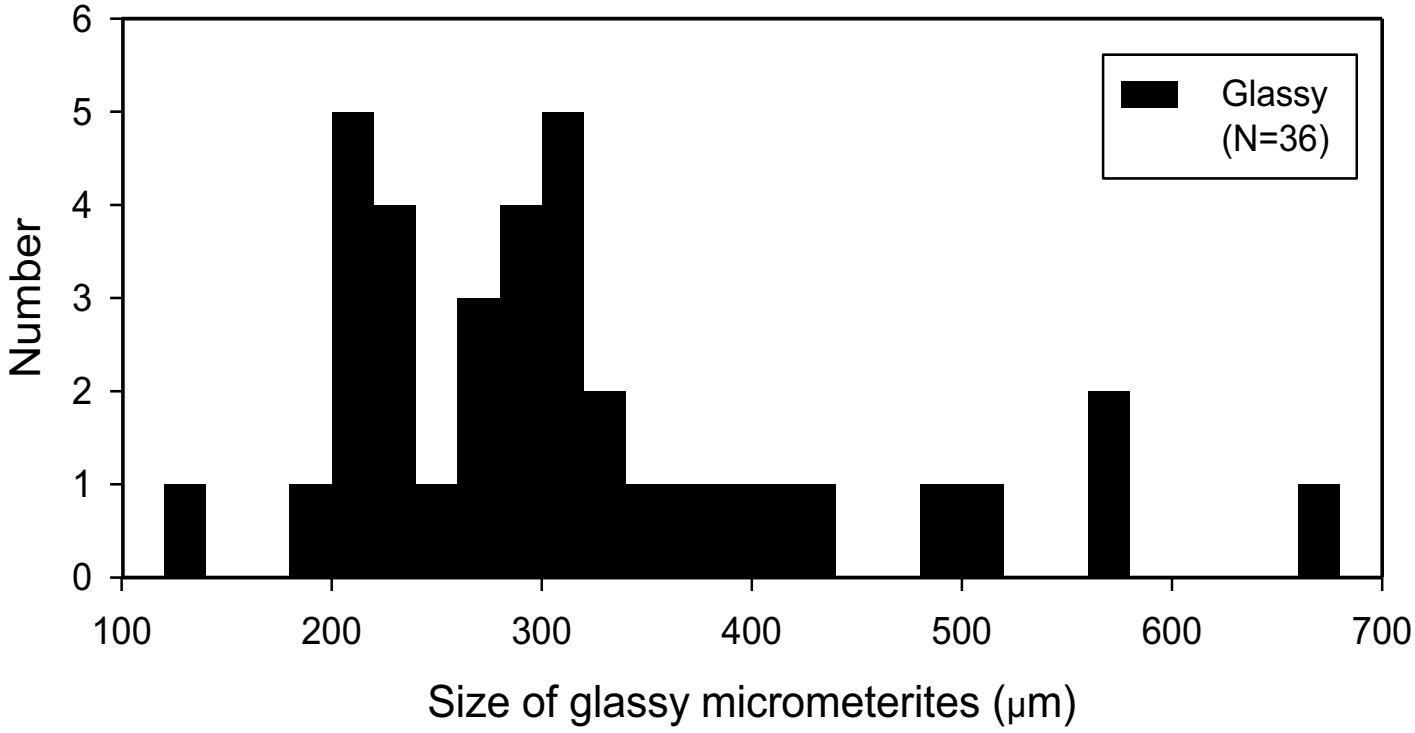
Glassy
(N=36)
Number
0
1
2
3
4
5
6
100
200
300
400
500
600
700
Size of glassy micrometerites (μm)

Fig. 14

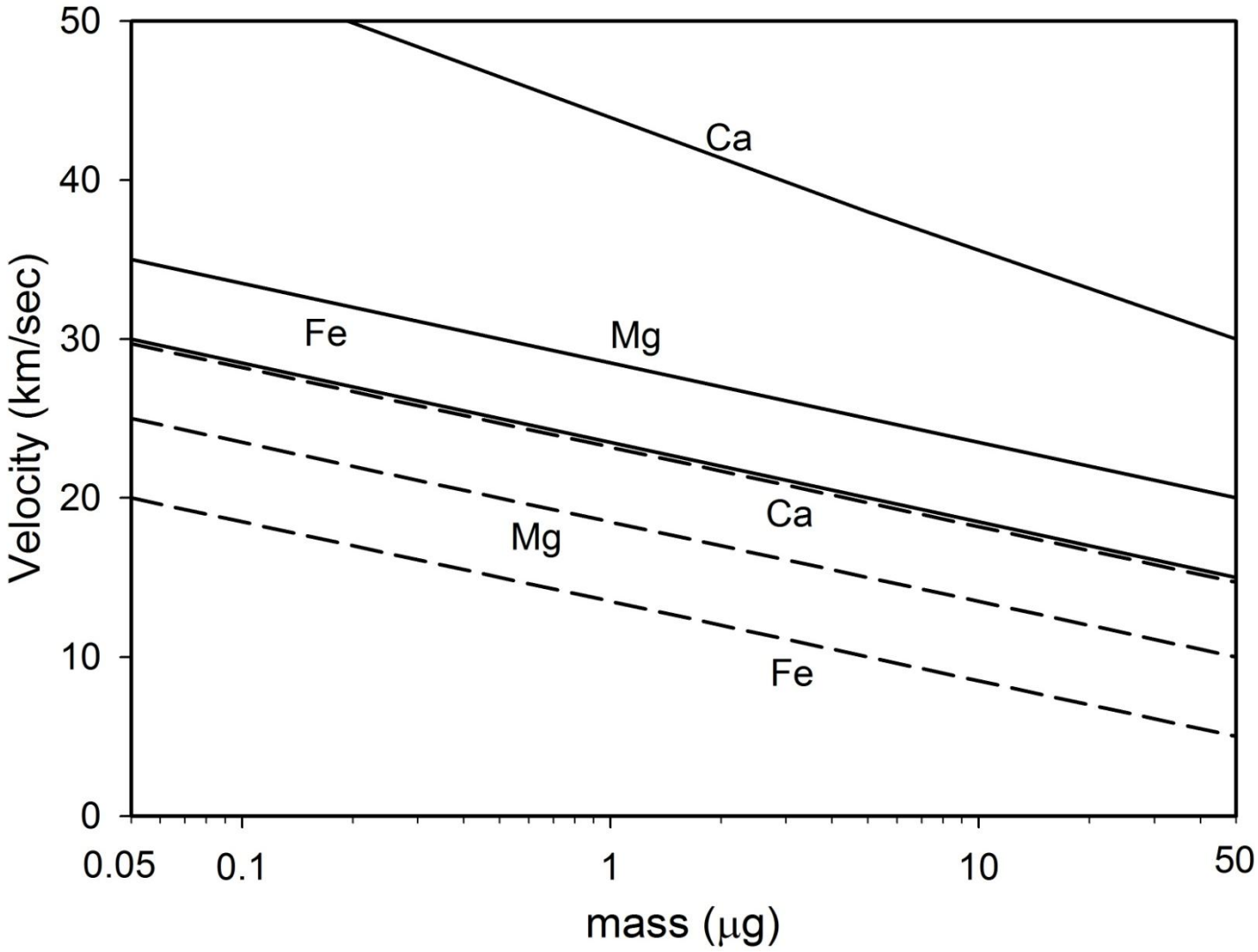
50
40
30
20
10
0
Velocity (km/sec)
Ca
Mg
Fe
Ca
Mg
Fe
0.05
0.1
1
10
50
mass (μg)

Fig. 15

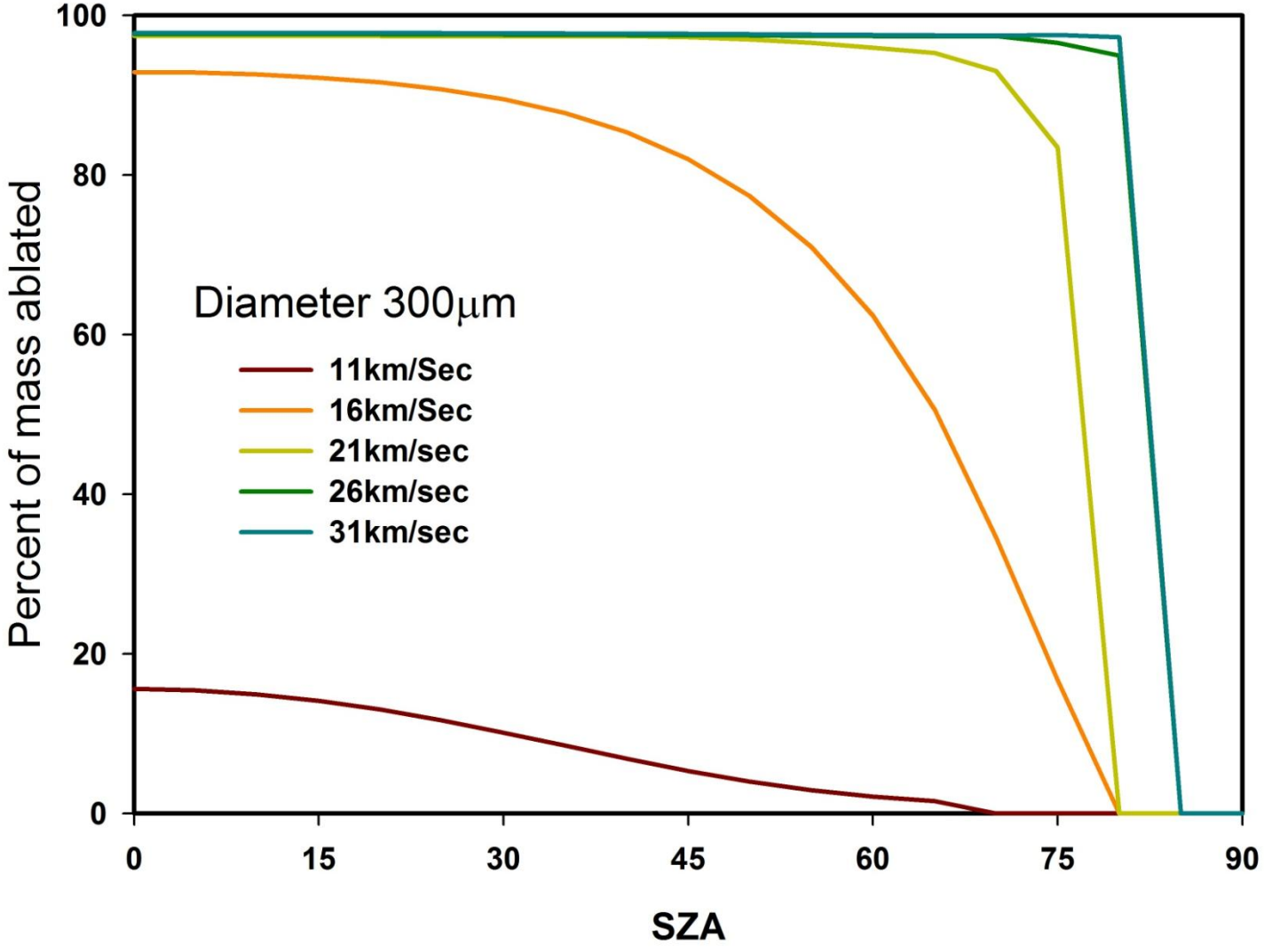
Percent of mass ablated
100
80
60
40
20
0
Diameter 300μm
11km/Sec
16km/Sec
21km/sec
26km/sec
31km/sec
0
15
30
45
60
75
90
SZA

Fig. 16

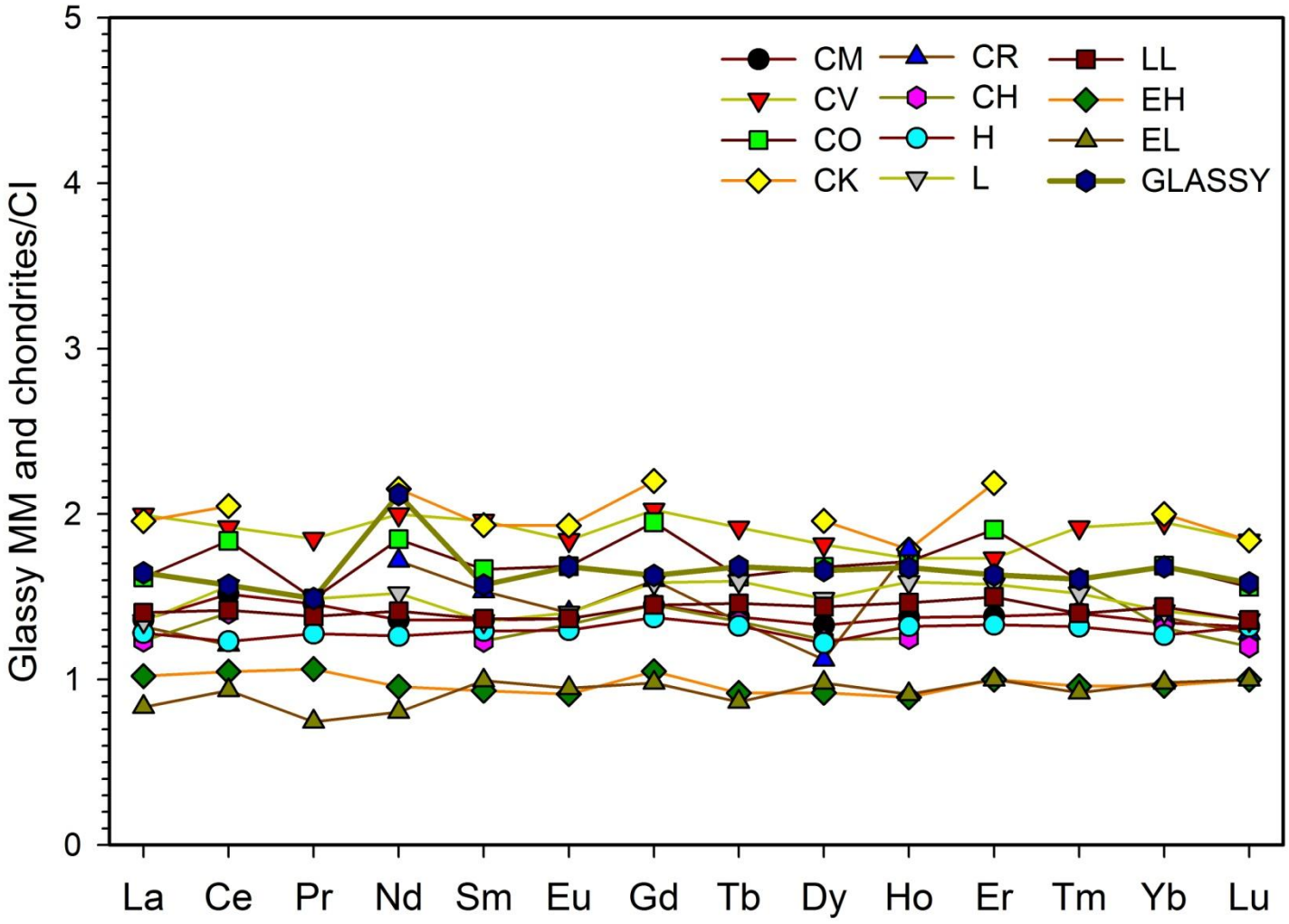
Glassy MM and chondrites/CI
5
4
3
2
1
0
CM
CR
LL
CV
CH
EH
CO
H
EL
CK
L
GLASSY
La
Ce
Pr
Nd
Sm
Eu
Gd
Tb
Dy
Ho
Er
Tm
Yb
Lu